Research Article

Check for updates

Mapping the micro-proteome of the nuclear lamina and lamina-associated domains

Xianrong Wong[1,3,4,*] , Jevon A Cutler[1,2,3,*], Victoria E Hoskins[1,2,3], Molly Gordon[5], Anil K Madugundu[1,2,6,7] , Akhilesh Pandey[1,2,6,7,8,9], Karen L Reddy[1,3,10]

The nuclear lamina is a proteinaceous network of filaments that provide both structural and gene regulatory functions by tethering proteins and large domains of DNA, the so-called lamina-associated domains (LADs), to the periphery of the nucleus. LADs are a large fraction of the mammalian genome that are repressed, in part, by their association to the nuclear periphery. The genesis and maintenance of LADs is poorly understood as are the proteins that participate in these functions. In an effort to identify proteins that reside at the nuclear periphery and potentially interact with LADs, we have taken a two-pronged approach. First, we have undertaken an interactome analysis of the inner nuclear membrane bound LAP2β to further characterize the nuclear lamina proteome. To accomplish this, we have leveraged the BioID system, which previously has been successfully used to characterize the nuclear lamina proteome. Second, we have established a system to identify proteins that bind to LADs by developing a chromatin-directed BioID system. We combined the BioID system with the m6A-tracer system which binds to LADs in live cells to identify both LAD proximal and nuclear lamina proteins. In combining these datasets, we have further characterized the protein network at the nuclear lamina, identified putative LAD proximal proteins and found several proteins that appear to interface with both micro-proteomes. Importantly, several proteins essential for LAD function, including heterochromatin regulating proteins related to H3K9 methylation, were identified in this study.

Introduction

DNA and proteins are highly organized within the eukaryotic cell nucleus. Sequestration of proteins into nuclear sub-domains and the higher order organization of chromatin itself have been implicated in the regulation of the genome (1, 2, 3, 4, 5, 6). Association of chromatin with the nuclear periphery, in particular, has been implicated in gene regulation, specifically correlating with repression of developmentally regulated loci (4, 7, 8). DamID (DNA Adenine Methyltransferase Identification), a genome-wide technique to identify nuclear lamina-proximal chromatin, has allowed the identification of lamina-associated domains (LADs) (9). These 100 kb to megabase (Mb) sized domains are enriched for genes that are transcriptionally silent and enriched in histone modifications indicative of facultative heterochromatin, such as histone H3 lysine 9 di/tri-methylation (H3K9me2/3) and histone H3 lysine 27 trimethylation (H3K27me3) (10, 11, 12, 13). Moreover, recent studies have highlighted that both H3K9me2/3 and H3K27me3 are involved in LAD organization (12, 13, 14, 15, 16). LADs represent a large fraction of the genome (30–50%, depending upon the cell type) and are highly correlated with the so-called heterochromatic "B-compartment," as identified by chromatin conformation capture assays (HiC) (13, 17 Preprint, 18 Preprint). Given their importance to cellular function and identity, it is important to understand how these large domains of heterochromatin are regulated, maintained, and formed to understand global genome regulation and organization. An important element of understanding LAD organization and function is identifying which proteins are present at LADs and the nuclear lamina.

In addition to H3K27me3 and H3K9me2/3, A-type lamins and the inner nuclear membrane (INM) proteins lamina-associated polypeptide β (LAP2β) and Lamin B receptor (LBR) have been implicated in organizing LADs (19, 20, 21, 22). The nuclear lamina is a proteinaceous network of type V intermediate filaments comprising A and B type lamins. These coiled-coil domain proteins provide a

[1]Department of Biological Chemistry, Johns Hopkins University of Medicine, Baltimore, MD, USA [2]McKusick-Nathans Department of Genetic Medicine, Johns Hopkins University School of Medicine, Baltimore, MD, USA [3]Center for Epigenetics, Johns Hopkins University School of Medicine, Baltimore, MD, USA [4]Laboratory of Developmental and Regenerative Biology, Institute of Medical Biology, Agency for Science, Technology and Research (A*STAR), Immunos, Singapore [5]Department of Cell Biology, Johns Hopkins University School of Medicine, Baltimore, MD, USA [6]Center for Molecular Medicine, National Institute of Mental Health and Neurosciences (NIMHNS), Bangalore, India [7]Institute of Bioinformatics, International Technology Park, Bangalore, India [8]Manipal Academy of Higher Education (MAHE), Manipal, India [9]Departments of Pathology and Oncology, Johns Hopkins University School of Medicine, Baltimore, MD, USA [10]Sidney Kimmel Cancer Institute, Johns Hopkins University School of Medicine, Baltimore, MD, USA

Correspondence: kreddy4@jhmi.edu
Jevon A Cutler's present address is Department of Pediatric Oncology, Dana-Farber Cancer Institute, Harvard Medical School, Boston, MA, USA
Xianrong Wong's present address is Laboratory of Developmental and Regenerative Biology, Institute of Medical Biology, Agency for Science, Technology and Research (A*STAR), Immunos, Singapore
Anil K Madugundu and Akhilesh Pandey's present address is Department of Laboratory Medicine and Pathology, Mayo Clinic, Rochester, MN, USA
*Xianrong Wong and Jevon A Cutler contributed equally to this work

structural scaffold at the INM, with the A-type lamins being shown to mediate LAD organization (12, 17 Preprint, 18 Preprint, 19). Longstanding efforts have been undertaken to map and characterize the local proteome of the nuclear lamina of the INM using INM preparations, co-immunoprecipitation and, more recently, BioID (Biotinylation Identification), a method for detecting proximal protein interactions in living cells (23, 24, 25, 26, 27). However, these efforts have exclusively focused on protein members of the INM/lamina as baits and have not measured the protein landscape of LADs themselves or the intersection of these proteome environments. To better understand these proximal protein compartments, we have leveraged the BioID system to study the "micro-proteome" of both LADs and the nuclear lamina using a multi-pronged approach. First, we have generated a chimeric protein comprising a modified promiscuous biotin ligase, BirA*, fused to the nucleoplasmic N-terminus of LAP2β to profile the INM/lamina proteome. We posit that this, coupled with other published proteomic profiling of the INM/lamina compartment, using other bait proteins, would

provide a more comprehensive overview of the INM/lamina (Fig 1A) (24, 25). Second, we have taken a novel approach combining the specificity of a DamID-based system to label LADs in live cells, the m6A-tracer system, and coupled this with BioID to characterize proteins proximal to LADs (Fig 1B and C) (16). Finally, we integrate these proteomic data with previous findings on lamin protein interactions to generate a comprehensive mapping of the LAD/lamina proteome interface.

Whereas a previous study used CRISPR-directed proximity-labeling approach to identify proteomes associated with repetitive sequences, this study represents, for the first time to our knowledge, a chromatin-directed-BioID strategy that is independent of identifying specific repetitive DNA sequences and targets a specific nuclear compartment (28). Herein, we identify the proteome of a chromatin compartment (LADs/B-compartment) by leveraging two proximity labeling techniques: BioID and DamID. In addition, by integrating published datasets, our new LAP2β interactome data, and our LAD directed proteome data, we have
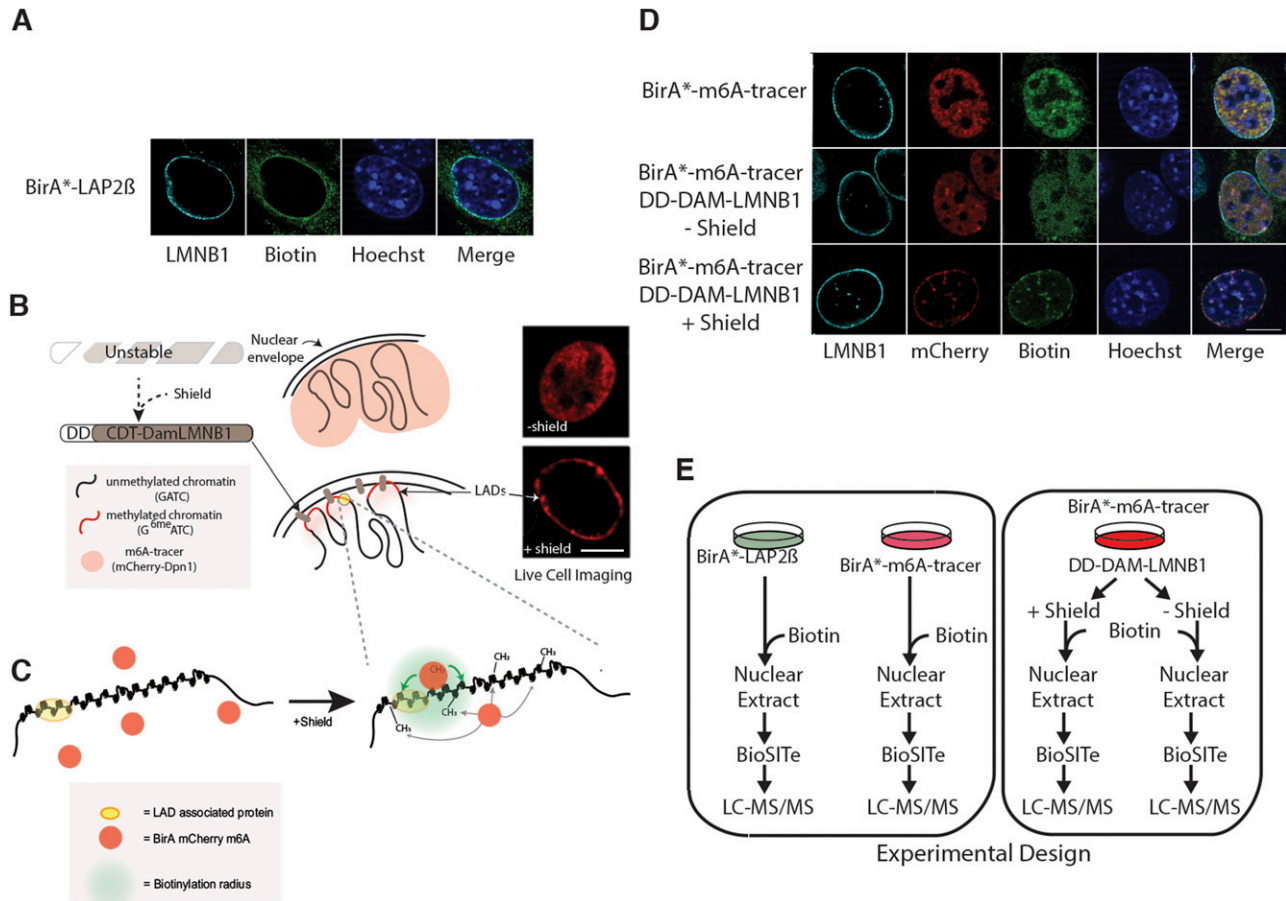

Figure 1. Strategy for investigating the nuclear periphery microproteomes.
(A) Representative images showing the biotinylated interactome of Lap2β (green) at the nuclear periphery in mouse embryonic fibroblasts (MEFs). **(B, C)** Pictorial representation of BirA* localization within the nucleus. Lamina-associated domains become methylated at GATCs upon Shield1 stabilization of Dam LmnB1, thereby recruiting BirA* mCherry m6A. Green shading in (C) depicts a putative biotinylation radius where available lysines on proximal proteins will be modified by BirA*. **(D)** Representative images showing the expected localization of the BirA*-m6a-tracer (red) and its biotinylated proteins (green) in the absence of DD-Dam LmnB1 (top row), in the absence (middle row) and presence (bottom row) of the shield ligand in MEFs. **(E)** Experimental workflow for mass spectrometry based BioID lamina associated domain microproteome analysis. MEF cells expressing BirA*-LAP2β, BirA*-m6a-tracer alone, BirA*-m6a-tracer/DD-Dam-LMNB1 plus/minus shield ligand were cultured with exogenous biotin then nuclei were extracted and Biotinylation Site Identification Technology (BioSITe) coupled to liquid chromatography/tandem mass spectrometry analysis was used to identify biotinylated proteins.

identified different interaction zones at the nuclear periphery, thus mapping the differential and overlapping microproteomes of the peripheral nuclear compartment. In zone 1, we identified proteins that appear to be restricted to the INM/lamina that do not interact with LADs. In zone 2 we identified proteins that interact with both LADs and the INM/lamina and these may comprise the "middle-men" required to organize the LADs to the nuclear lamina. Finally, in zone 3 we identify proteins that are restricted to LADs, many of which are involved in regulating histone H3 lysine 9 methylation (H3K9me2/3) and cell cycle regulation.

Results

Establishment of BioID system to map the local proteomes at the nuclear periphery

The BioID system was initially developed using the Lamin A protein as the bait allowing a robust interactome of this insoluble protein (25). The BioID system relies on an engineered biotin ligase, BirA* which, when expressed in cells, has a small practical in vivo biotinylation radius of ~10 nm (29), thus labeling lysines on both proximal and directly interacting proteins. BioID, among other methods, has been used to analyze the local proteome of the INM using Lamin A/C proteoforms, Lamin B1 (LMNB1), SUN domain-containing protein 2 (SUN2), and nuclear pore complex (NPC) members as baits (23, 25, 29, 30 Preprint). To expand on these efforts and to focus on an INM protein implicated in LAD organization, we chose to identify vicinal proteins of the LAP2β in a BioID study. The LAP2β protein results from alternative splicing of the gene thymopoietin (TMPO) and was initially observed in nuclear envelope isolations and shown to bind lamin proteins (31). LAP2β is an integral INM protein that is thought to link the nuclear membrane to chromatin and also to regulate transcription factor functions (32). LAP2β is a member of the LEM (Lap2-Emerin-Man1) domain family of proteins and contains a LEM domain as well as a LEM-like domain, both of which have been thought to mediate interactions between protein/DNA complexes with the lamin binding region. To leverage the BioID system for analysis of the LAP2β proximal interactome we have tagged the nucleoplasmic N terminus with BirA* (Fig 1A).

BioID is closely related to the DamID technique in that both techniques rely on in-cell labeling of proximal molecules (9). In DamID, instead of modifying proteins, a Dam-X fusion protein modifies interacting DNA segments by methylating GATC stretches (G^{me}ATC). This modification can be used to isolate interacting DNA regions by cutting with the methyl-specific restriction enzyme, DpnI. In a typical DamID experiment, these fragments are amplified and subjected to DNA sequencing to generate genomic maps of interacting regions. The m6A-tracer system is an adaptation of the DamID technology for visualizing LADs in live-cell imaging (16). Our variation of the m6A-tracer system relies on the demarcation of LADs by an inducible and interphase restricted methylation of LADs underlying the nuclear lamina by Dam-LMNB1 (DD-Dam-hCdt-LMNB, Fig 1B). The inducibility and restriction to interphase labeling is conferred by the destabilization domain (DD) (16, 17 Preprint, 33 Preprint) and the Cdc10 dependent transcript 1 (hCdt) domains (17 Preprint, 33 Preprint, 34), respectively, with the

DD domain causing degradation of Dam-LMNB1 in the absence of the shield ligand and the hCdt domain causing its degradation in all phases of the cell cycle with the exception of G1. Detection of the G^{me}ATC-marked DNA (the LADs) is performed by the m6A-tracer, a catalytically inactive G^{me}ATC binding domain of the DpnI enzyme, fused to a fluorescent protein (such as mCherry) (16, 17 Preprint, 33 Preprint).

To map the local proteome of the INM and LADs we generated three independent MEF cell lines expressing either BirA*-Lap2β (to map the INM/lamina, Fig 1A), BirA*-m6A-tracer alone (control), or BirA*-m6A-tracer with DD-Dam-LMNB1 (to map the LAD proteome) (Fig 1D). These cells were grown in the presence of exogenous biotin to enable efficient labeling of proximal proteins by BirA*. Cells harboring both BirA*-m6A-tracer and DD-Dam-LMNB1 constructs were split into two sets of cultured cells, one in the presence of the shield ligand and one without, as an additional control for the LAD proteome experiments (Fig 1E). To remove cytoplasmic contamination and limit our interrogation to the nucleus, a crude nuclear extraction preparation was performed on all cells. To detect biotinylation on candidate proteins, we used Biotinylation Site Identification Technology (BioSITe) and liquid chromatography-tandem mass spectrometry (LC-MS/MS) (Fig 1E) (35).

Analysis of the LAP2β interactome using BioID

To identify proximal proteins of LAP2β, we used BirA* tagged LAP2β (BirA*-Lap2β) containing cells (Fig 1D). As a background control we used the BirA*-m6A-tracer construct expressed alone, without the presence of the DD-Dam-LMNB1 construct, which resulted in diffuse nuclear localization (red signal, Fig 1B) and subsequently similar biotinylation pattern (green signal, Fig 1D). A previous study using LAP2β tagged with BirA* found that the expressed protein was mislocalized to the ER and cytoplasm. This is not very surprising because it has been previously shown that over-expression of LEM domain proteins leads to their accumulation in the ER and cytoplasm, and such mis-localization occurs with disease variants of lamin proteins as well (31, 36, 37). We therefore sought to express our protein at low levels to preserve normal localization (Fig S1). In addition, this low expression ensures minimal disruption to normal function of Lap2β and its partners and minimizes cellular stress due to overexpression (and mislocalization). To detect where our low-expressing BirA*-Lap2β construct localized, we measured biotinylation signals using immunofluorescence on fixed MEFs expressing BirA*-Lap2β. As evidenced by the strong nuclear rim staining, we did not observe any gross mislocalization of LAP2β (Fig 1B). Some evidence of ER and mitochondrial expression is evident by the streptavidin signals, and this is to be expected because LAP2β transits the ER and there are endogenously biotinylated proteins in mitochondria. Therefore, as an additional step to maximize bona fide nuclear interactions, we performed a nuclear extract before protein isolation. Although this extra step may result in the loss of some true nucleoskeletal–cytoskeletal interactions, it increases the rigor in detecting nuclear interactions. The correct localization of our LAP2β-BirA* (Fig 1B), its low expression (1–2% of endogenous levels of LAP2β, Fig S1) that obviates perturbations to the INM due to overexpression of a key INM protein, and a nuclear

isolation step allowed for enriched detection of Lap2β-proximal proteins.

Using BioSITe to detect biotinylated proximal proteins in our BioID screen we identified 334 total biotinylation sites in the BirA*-LAP2β containing cells and 684 sites in the BirA*-m6A-tracer alone containing cells (control). MS1 level quantitation was applied to obtain relative abundance differences between duplicate LC-MS/MS analyses of BirA*-LAP2β and BirA*-m6A-tracer cells. Replicate agreement was plotted (Fig 2A) and proteins enriched >2-fold were considered for LAP2β proximity/interaction (Table S1). Among the proteins enriched over control were expected and known interactors of LAP2β: LEM-domain containing protein 3 (MAN1), Emerin (EMD), and Lamins A and B1/2. Other known nuclear lamina proteins that were biotinylated were SUN domain contain proteins 1 and 2 (SUN1 and SUN2), LBR, and many NPC members (4, 38).

In an effort to rank the biotinylated proteins enriched over the control, in terms of potential closer proximity, we calculated the degree of biotinylation (number of biotinylated lysines/total lysines) and ordered proteins from greatest to least (Fig 2B) (35). We detected that the bait LAP2β has the greatest degree of biotinylation followed by Emerin, MAN1, LBR, LMNB1/2, LMNA, and SUN1/2. We hypothesize that these proteins represent the most

proximal and/or abundant interactors of LAP2β on the nucleoplasmic side of the INM.

To verify that our list of proteins was in fact enriching for nuclear envelope proteins we also submitted detected biotinylated proteins to cell component analysis using the Enrichr Web-based analysis tool (39). Some of the top cellular component terms included nuclear periphery (GO:0034399), nuclear lamina (GO:0005652), and nuclear matrix (GO:0016363) (Fig 2C). To further examine if our data were consistent with previous studies, we benchmarked our data on four published studies of nuclear envelope interactomes (23, 24, 25, 29, 30 Preprint, 40, 41) (Table S3): (1) Bar et al combined a novel antibody based proximity labeling strategy and a meta-analysis of many Lamin A and B interactome studies that included methods such as BioID, yeast two hybrid, and co-immunoprecipitation to obtain a list of higher confidence "true" proteins at the NE/lamina. (2) Kim et al used BioID on many NPC members to build out the proximal proteins within the NPC and (3) Xie et al used BioID on both A-type lamins. (4) Birendra et al also used BioID to examine the interactomes of Lamin A and Sun2. We found 36 proteins to be overlapping between the union of these four studies (protein must have been observed in three of the four studies) and our LAP2β interactome analysis (Fig 2D), including
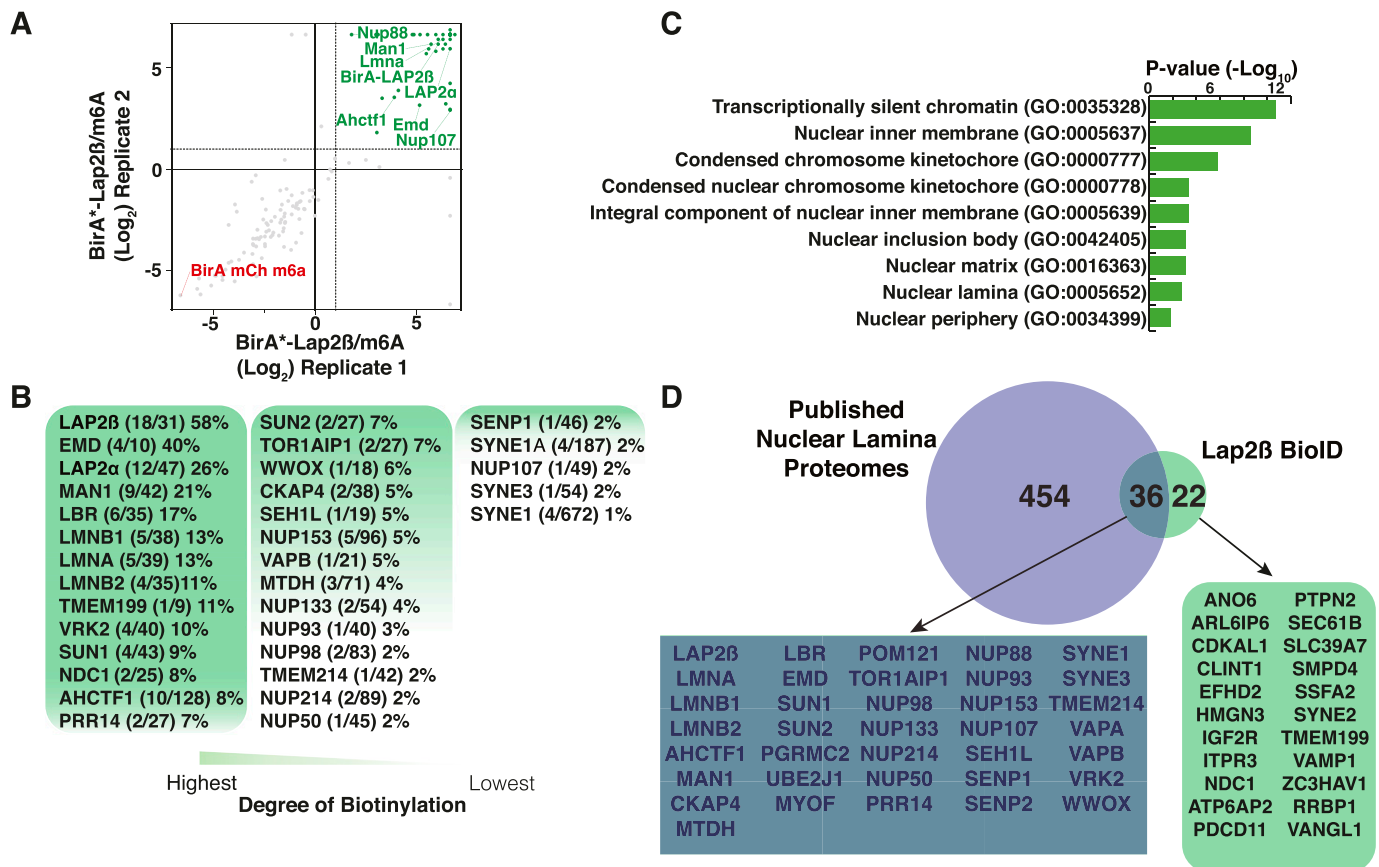

Figure 2. LAP2β BioID interactome.
(A) Plot of replicate runs of MS1 level quantitation ratios of mass spectrometry identities of BirA*-LAP2β over BirA*-m6A-tracer alone containing cells. **(B)** Degree of biotinylation analysis of LAP2β interactome study. **(C)** Gene set enrichment analysis of LAP2β proximal proteins. **(D)** Venn diagram of current LAP2β BioID analysis and published nuclear lamina proteome analyses.

most of our proteins showing the highest degrees of biotinylation. We believe that these proteins represent very high confidence nuclear envelope proteins.

We do, however, note the representation of ER proteins and nuclear pore proteins (NUPs) in our LAP2β data set which includes vesicle-associated membrane protein-associated protein B (VAPB) and nucleoporin NDC1 (NDC1). We hypothesize that this could be due to the NPC presenting itself as a kinetic bottle-neck for the relatively large BirA*LAP2β and therefore, longer residence times in the ER and NPCs. In addition, notably absent from our Lap2β interactome analysis is Barrier to Autointegration factor (BANF1) which is a known interactor of Lap2β, as well as HDAC3, another putative interactor (42, 43, 44). We hypothesize that the small size of BAF (~10 kD) makes detection of this protein by mass spectrometry based approaches particularly challenging. It is also important to emphasize that BioID is a label transfer technique and hence, the biotinylation of potentially transient interactors such as HDAC3, coupled with limited material because of the sub-physiological expression level of BirA*-LAP2β, it is possible that some of these might have been missed by our analysis.

Given that LAP2β contains a transmembrane domain which is localized within the INM, we next examined our data for transmembrane domain-containing proteins. We observed that 34 of the 58 LAP2β proximal proteins contained a transmembrane domain (Table S1). It has been shown that membrane topology can be predicted with biotinylation site level data, which BioSITe provides (35). Many of these proteins exhibited biotinylation on areas of the protein consistent with lumen/nucleoplasmic annotated topology (Table S1). Interestingly, 18 of these proteins also have subcellular annotation for the ER, including VAPB, CKAP, and TMEM214, which could indicate unknown nuclear localization and function; however, it is also possible that these proteins are part of the ER trafficking of LAP2β to the nucleus (45).

LAD-directed BioID using the m6A tracer system

Having identified and refined the proteome at the lamina, we next asked if we could discriminate proteins that are proximal to LADs and their relationship with the nuclear lamina network using our m6A tracer system, which is built off the sequencing technique DamID. In DamID, DNA adenine methyltransferase (Dam) derived from *Escherichia coli* is fused to a DNA-interacting protein (9). Dam adds methyl groups to adenines in the vicinity of the fusion protein, thereby marking the interaction sites on the proximal DNA segments (G^meATC) which can be cut with the G^meATC-specific restriction enzyme *DpnI*. Fragments are then subjected to ligation-mediated PCR and deep sequencing. Using Dam-Lamin B1 and Dam-only (normalizing control) to mark DNA, the resulting data identify regions of DNA associating with the nuclear lamina, LADs, expressed as a relative enrichment ratio: log$_2$ (Dam-Lamin/Dam only). The m6A-tracer system is an adaptation of the DamID technology for visualizing LADs in single-cell live imaging (16). This system relies on the demarcation of LADs by an inducible Dam-LMNB1 (in this study, DD-Dam-hCdt-LMNB1), the expression of which can be exogenously controlled via Shield1 ligand masking of the DD and also restricted to interphase by hCdt1 dependent degradation in all phases of the cell cycle except G1. The detection

of this marked DNA (the LADs) is then performed by the m6A-tracer, a catalytically inactive G^meATC-binding domain of the *DpnI* enzyme, fused to a fluorescent protein (BirA*-m6A-tracer in Fig 1B) (34, 46, 47, 48). The DD domain prevents accumulation of the fusion protein via proteasomal degradation in the absence of shield ligand (Fig 1B–D) (49, 50). Upon introduction of shield ligand, the protein is stabilized, enabling the DD-Dam-hCdt1-LMNB1 protein to methylate LADs during G1.

To identify LAD-proximal proteins, we compared biotinylated peptides from cells harboring DD-Dam-LMNB1 and BirA*-m6A-tracer with (marks LAD-proximal proteins) or without (background control) shield ligand. LAD-specific interactions were determined to be >1.6-fold average ratio between replicates (replicate agreement is plotted in Fig 3A) of plus over minus shield ligand (i.e., recruited to LADs over background). Using BioSITe to detect proximal proteins, we found 1,179 biotinylation sites in the plus shield condition and 1,128 in the minus (Table S2) (35). Using this approach to map the proteome of LADs, we were able to identify three major classes of proteins enriched in the plus shield condition: INM proteins, cell cycle related, and DNA-binding/chromatin proteins (Fig 3B and C).

Specifically, to better understand the 112 LAD-proximal proteins that were enriched over our minus shield control, we submitted these proteins to pathway analysis using the Enrichr Web-based pathway analysis (Fig 3B) (39). Of the most significantly enriched biological processes, many were processes in negative regulation of DNA transcription and cell cycle–related pathways. Examples of the latter include: mitotic sister chromatid cohesion and segregation, regulation of mitotic metaphase plate congression. Notable cell cycle–related genes include many members of the cell division cycle–associated protein family, including 2 (CDCA2), 5 (CDCA5), 7 (CDCA7), and 8 (CDCA8) and many kinesin family members such as 4A (KIF4A), 18B (KIF18B), 20A (KIF20A), and 20B (KIF20B). We also observed that many microtubule/spindle attachment proteins related to the kinetochore including the serine/threonine kinase that regulates segregation of chromosomes during mitosis Aurora kinase B (AurkB), nucleolar and spindle associated protein 1 (Nusap1), regulator of chromosome condensation 2 (RCC2), microtubule nucleation factor (TPX2), sister chromatid cohesion protein (PDS5), and inner centromere protein (INCENP). In addition, the replication timing factor Rif1, was identified as LAD-interacting, in agreement with previous studies (51, 52).

As expected, another highly represented class of proteins enriched on LADs were proteins of the INM. These included many known INM proteins such as LAP2β, MAN1, Emerin, Lamins A and B1/2, LBR, and SUN1 (Fig 3C). Strikingly, NUP proteins were not enriched in the LAD proteome, suggesting that these chromatin domains are indeed not proximal to NPCs, in agreement with cytological data.

LADs are particularly enriched in chromatin modifying and binding proteins

As mentioned above, one of the major classes of proteins enriched on LADs were involved in negative regulation of transcription. Specifically, many of the identified proteins have roles in the establishment/regulation of H3K9 methylation or bind to H3K9 methylated histones, such as heterochromatin protein 1 α and β
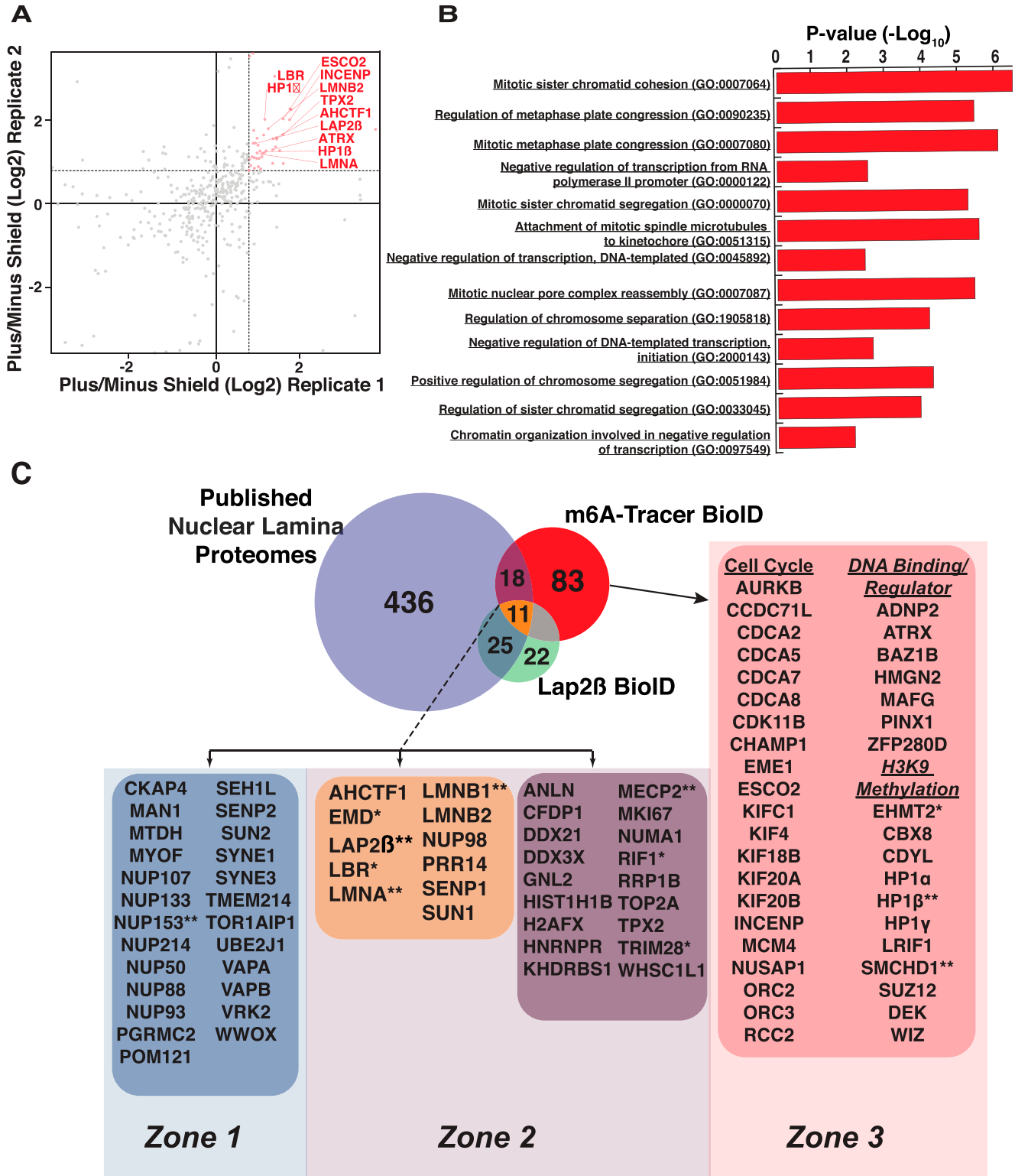
Figure 3. Lamina associated domain (LAD) microproteome analysis.
(A) Plot of replicate runs of MS1 level quantitation ratios of mass spectrometry identities of BirA*-m6A-tracer/DD-Dam-LMNB1 plus shield over minus shield ligand. **(B)** Gene set enrichment analysis of m6A-tracer BioID LAD proteome. **(C)** Integrative venn diagram of published nuclear lamina proteomic analyses, our current LAP2β BioID interactome analysis and the LAD-ome analysis. Proteins marked * have been validated by various groups, including ours. The experiments and results are summarized in Table 1. Proteins marked ** have been bioinformatically validated in-house. Note: not all proteins in these overlaps are shown for display purposes. Please see Table S3 for a full list of proteins. Data from C57BL/6 3T3-derived WT MEFs.

(HP1α and HP1β), polycomb repressive complex 2 subunit Suz12, TRIM28 (Kap1), SMCHD1, PRR14, and DEK (Fig 3C). Of particular interest were the abundance of LAD-interacting proteins involved in establishment and maintenance of heterochromatin, specifically euchromatic lysine methyltransferase 2 (EMHT2) and its binding partners chromodomain Y like (CDYL) and the transcription factor widely interspaced zinc finger motifs (WIZ). These proteins have been shown to facilitate mono- and dimethylation of H3K9.

Finally, we also observed many additional chromatin modifying and DNA binding proteins such as AT-hook containing transcription factor 1 (AHCTF1, also known as ELYS, which has also been implicated as a bona fide NPC protein (53, 54)), ATRX chromatin remodeler (ATRX), MECP2, tyrosine-protein kinase BAZ1B (BAZ1B), high mobility group nucleosomal binding domain 2 (HMGN2), and PIN2/TERF1 interacting telomerase inhibitor 1 (PINX1) (53, 55, 56, 57, 58). We also identified a few transcription factors not known to be involved in heterochromatin such as MAF BZIP transcription factor G (MAFG), zinc finger protein 280D (Zfp280d), and ADNP homeobox 2 (ADNP2).

Integration of laminome and LADome data identify unique and overlapping micro-proteomes

We next sought to determine the overlapping proteomes between the nuclear lamina and LADs. We focused on using existing data and our new Lap2β proteome to maximize potential proteins interacting with chromatin. There were 54 proteins that overlapped between the published laminome data and our Lap2β proteome or the m6A-tracer LAD proteome (Fig 3C, Venn diagram overlaps). Importantly, the well-known nuclear lamina proteins such as LBR, LMNA/C, LMNB1, and SUN1 all showed enrichment on LADs as well (Fig 3C, yellow box). In contrast, whereas the published laminome and Lap2β showed interactions with NPCs (NUPs, Fig 3C, blue box), these were largely missing from the LAD interactome data. This finding supports cytological and DamID studies, suggesting that the chromatin underlying the NUPs is more euchromatic and distinct from the peripheral heterochromatin that comprises LADs.

In total, we identified 29 proteins, including MECP2, AHCTF1 (also known as ELYS), and PRR14, that were found to be biotinylated in the BirA*-m6A-tracer experiment that were also detected in the published nuclear lamina interactomes and/or our Lap2β interactome (Fig 3C, purple and yellow boxes). These are potential candidates for proteins that are at the interface of the INM and LADs, perhaps linking them together and regulating dynamic LAD organization (4).

The 47 proteins detected only in the LAP2β-BioID experiment, as well as most proteins in the published laminome data that are not LAD-enriched (Fig 3C, blue box and light and dark blue Venn regions), likely represent more INM proximal proteins that do not interact with and are farther from the underlying chromatin (LADs). These include the previously described NUP proteins. Other examples include, Progesterone Receptor Membrane Component 2 (PGRMC2), Torisin-1A-interacting protein 1 (Tor1aip1), Myoferlin (MYOF), transmembrane protein 214 (TMEM214), metadherin (MTDH also called protein LYRIC), cytoskeleton associated protein 4 (CKAP4), vesicle-associated membrane protein-associated protein B/C (VAPB); these are all transmembrane-containing proteins that

may not have large enough nucleoplasmic domains to be in proximity to the LADs, and, for the Lap2β proximal transmembrane proteins, could also represent transient interactions from transit through the ER. Nonetheless, these proteins appear to be more distal to the underlying LAD chromatin. Interestingly, SYNE1 and SYNE3 which code for Nesprins 1 and 3 are classified in this group. Although there is evidence that nucleoplasmic nesprins exist (59, 60), it is also possible that these proteins were biotinylated en route to the INM.

Eighty-three proteins were identified as associating *uniquely* with LADs (Fig 3C, red Venn region and pink box). Because the LADs and the lamina are in such close proximity, we were surprised to find such a clear distinction between the LADome and the laminome. The LAD-specific proteins include the previously described chromatin modifier complexes such as EHMT1/2, cell cycle regulators and chromatin interactors. This is particularly interesting, given the recent evidence that chromatin state directs LAD organization (12, 14, 15, 16, 17 *Preprint*, 18 *Preprint*). These data suggest, and support previous findings, that these regions are enriched for chromatin complexes that initiate and maintain a heterochromatic state (10, 12). These data also support a model in which chromatin state is established independently from association of these chromatin domains with the lamina because these proteins do not interact with the INM/lamin directly (15, 17 *Preprint*).

Validation and other supporting data

To our knowledge, this presents the first comprehensive characterization of the local proteome associated with LADs. Many of the proteins identified have already been extensively validated, with some of these validations corroborating the placement of the proteins in specific interaction groups: INM/lamina, interface, or chromatin restricted. Published and new validation experiments and data that directly show association with the INM/lamina and/or involvement in LAD establishment/maintenance have been summarized and compiled in Table 1.

Proteins at the INM/lamina that do not interact with LADs
Proteins at the INM/lamina that showed no enrichment likely represent nuclear envelope proteins that are spatially removed from LADs and would therefore be restricted from interacting with LAD chromatin. To test this supposition, we interrogated the interaction of one such protein, Nup153, with LADs using publicly available data (Fig 4) (10, 61). Nup153 has previously been shown to interact with chromatin, but our data suggest that this protein is excluded from LAD chromatin domains. We find that most Nup153 interactions with chromatin occur outside of LADs and, intriguingly, Nup153 peaks that appear to be within LADs (at a gross scale) coincide with regions that have low Lamin B1 signal, which we have previously termed DiPs (Depleted in Peripheral signal (18 *Preprint*); Fig 4). Interestingly, these DiPs correlate with active transcription start sites and enhancers, with a distinct and discrete switch from the inactive B to the active A chromatin compartment. These combined data support our integrated BioID data which suggest that the Nup153 interactions with chromatin at the lamina are more distal to LADs (Fig 4).

Table 1. Table detailing experiments and results from published work directly validating protein hits from our BioID study.

Protein	Experiment	Results
Lap2b (20) (Fig 5)	• DamID	• *Lap2b DamID show traces almost identical to LMNA DamID (molecular association with LADs)*
Emerin (10)	• DamID	• EMD DamID profiles are virtually identical to LmnB1 DamID (molecular association with LADs)
LBR (19)	• Developmental characterization	• LBR is genreally expressed more predominantly in progenitor cells switching to Lamin A/C later in development
	• Functional characterization of chromatin in Lamin A/C and LBR double KO mice	• All post mitotic cells in Lamin A/C; LBR double knockout mice exhibit loss of peripheral chromatin and inverted chromatin configuration (histological)
	• Ectopic LBR expression in photoreceptor rod cells in mice	• Inverted chromatin configuration found in rod cell nuclei can be counteracted with ectopic LBR expression
Lamin A/C (12, 17 *Preprint*, 18 *Preprint*, 19, 20, 21, 22, 65; Fig 5)	• DamID	• *LMNA DamID profiles are virtually identical to LmnB1 DamID (molecular association with LADs)*
	• Knockdown and Immunofluorescence	• Fragments that by default localized at the periphery were found to have loss peripheral localization.
	• Knockdown studies and 3D-immunoFISH	• Disrupted association of LADs with the nuclear periphery AND overall chromosome territorial architecture
	• Developmental characterization of expression	• LMNA expressed more predominantly in more differentiated cells (compared with LBR)
	• Histological characterization of chromatin in KO mice	• Removing Lamin A/C from cells lacking LBR expression resulted in loss of LADs and an inverted chromatin organization
		• All post mitotic cells in Lamin A/C, LBR double knockout mice exhibit the inverted chromatin organization.
Rif1 (51, 52)	• Electron microscopy	• Gold labelled beads (as readout Rif1 localization) on heterochromatin at the periphery
	• Nuclear subfractionation.	• Found in DNAse-resistant as well as salt-resistant nuclear fraction
	• Knockout affected replication timing	• Affected replication timing and nuclear architecture
	• Rif1 ChIP	• Correlates with LADs
	• Immunofluorescence	• Localizes at the nuclear periphery
	• Co-Immunoprecipitation	• Rif1 immunoprecipitates LmnB1
MeCP2 (55, 62, 66, 79, 104; Fig 5)	• ChIP	• Highly correlated with LAD traces
	• Immunofluorescence and colocalization studies	• MeCP2 and LBR colocalizes at the nuclear periphery
	• Biochemical fractionation of nuclei	• MeCP2 exists in the MNase and salt-resistant nuclear pellet
	• Coimmunoprecipitation assays	• MeCP2 coimmunoprecipitates LBR and vice versa
	• Bimolecular Fluorescence Complementation	• MeCP2 and LBR interacts at the nuclear periphery

Table 1. Continued

	Protein	Experiment	Results
TRIM28	TRIM28 (KAP1) (66, 68, 69)	· Coimmunoprecipitation	· Interacts with Lamin A
		· Ectopic recruitment to genomically integrated transgene via hormone responsive KRAB zinc finger proteins	· Acts as obligate corepressor of hormone responsive KRAB zinc finger proteins; represses genes by associating with HP1 and SETDB1
RRP1B	RRP1B (66, 70)	· Bimolecular Fluorescence Complementation	· RRP1B interacts with Sun2 at the nuclear periphery
		ChIP-reChIP	· Interacts with Trim28 and HP1
PRR14	PRR14 (63, 64, 73, 98)	· Yeast 2 hybrid	· PRR14 is a binding partner for HP1α
			· N-terminal 135 amino acids (containing NLS- and HP1-binding site) sufficient for nuclear peripheral localization
		· Functional and deletion mapping coupled to immunofluorescence	· Mutation of HP1-binding motif disrupts nuclear peripheral targeting
			· Central region required for lamina localization
		· Knockdown studies	· Decreased HP1α at the nuclear periphery upon PRR14 knockdown
			· LmnA/C knockdown affected PRR14 localization at nuclear periphery
		· Cell cycle studies by immunofluorescence	· Assemble on chromatin at anaphase
EHMT1	EHMT2/G9a (12, 13, 14, 15, 16, 17 *Preprint*, 18 *Preprint*)	· Drug (BIX-01924) inhibition of G9a and/or siRNA against G9a followed by DamID or immunofluorescence	· Fragments that by default localized at the periphery were found to have loss peripheral localization (by immunofluorescence) and association (by DamID)
			· Endogenous LADs were also shown to have a lower relative nuclear association when compared with non-treated or control-treated samples.
		· G9a overexpression	· Increased relative nuclear lamina association of LADs compared with non-treated or control-treated samples.
		· Drug inhibition of G9a followed by 3D- or immunofluorescence	· Disrupted association of LADs with the nuclear periphery AND overall chromosome territorial architecture
HP1	CBX1 (HP1β) (72; Fig 6)	· DamID	· *Highly correlated with LAD traces*
			· Important for X-chromosome structure
SMCHD1	SMCHD1 (72; Fig 6)	· DamID	· *Highly correlated with LAD traces*
			· Important for X-chromosome structure

References and figures describing the role of these proteins at the INM/lamina or on LADs are in parentheses.

Proteins that bind the INM/Lamina network and LADs—the "middlemen"

Proteins that interface the INM/Lamina and LADs are candidates for linking them together and regulating dynamic LAD organization (4). This group is composed of both INM/Lamina proteins and chromatin binding proteins. It is hardly a surprise that lamin proteins fall into this category as they have been shown to interact with LADs and to be important for their localization to the nuclear periphery (Table 1 and Fig 5). In addition to the lamin proteins, some INM proteins were also identified as spanning the INM/lamina and interacting with chromatin. For instance, LBR has previously been shown to interact with chromatin and is required for normal chromatin domain organization in early development (Table 1, 19) as well as

Emerin, a LEM domain protein, displays interactions with chromatin, as measured by DamID, which are highly correlated with LADs (10). In addition, both LBR and emerin have been identified in multiple BioID and biochemical experiments to interact with the same lamin network (10). These combined data support our findings here that these proteins span the lamina network and chromatin interface. We find that the LEM domain protein Lap2β also falls into this category. We note, however, that we failed to detect another LEM domain protein, Man1, in our LAD proteome. We speculate that this is due to a lower abundance of this protein, but this could also be because it does not have lysine residues proximal to LADs. Nonetheless, Lap2β has been shown, through multiple experiments, to interact with the lamina and INM
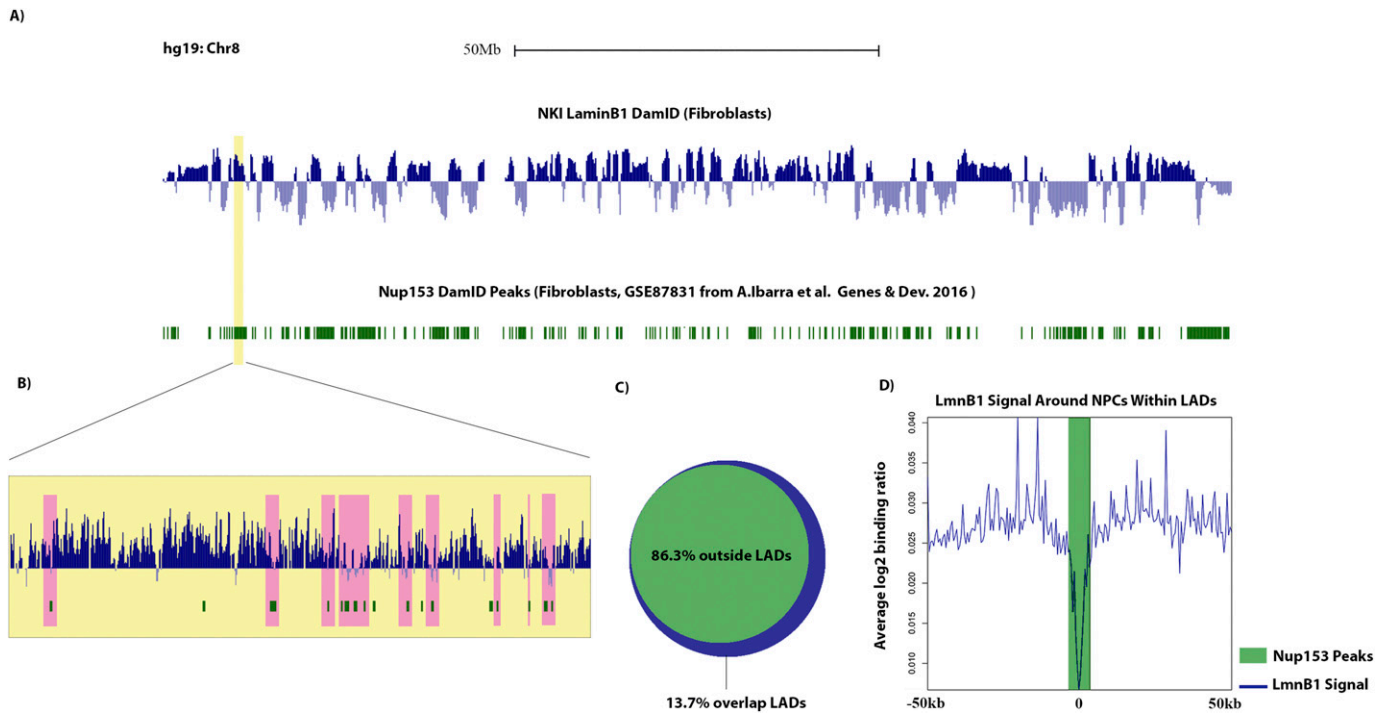
Figure 4. Nup153 interacts with lamins, but not LADs (Zone 1). (A) Log$_2$ ratio plots from human fibroblasts (hg19 build) chr 8 of LmnB1 DamID (blue) and Nup153 DamID peaks in green (10, 73). **(B)** Inset shows a magnified view of a lamina-associated domain (LAD) that appears to be highly dense with Nup153 binding sites. **(C)** Venn diagram showing the percentage (in base coverage) of Nup153 distribution relative to LADs. **(D)** LmnB1 profile anchored at all LAD-Nup153 peaks (the 13.7% that are found within LADs) centers. Line graphs represent the average trend across all such Nup153 peaks.

network. In addition, several studies have suggested that this protein is important for LAD organization and regulation (12, 20). We therefore decided to interrogate the interaction of Lap2β with LADs to verify that this protein indeed interacts across the INM/chromatin interface, as our BioID data suggest, and to test the breadth of such interactions. Using a DamID approach, we find that Lap2β interaction with chromatin occurs on LADs; the Lap2β interaction signatures are virtually identical to LADs (Figs 5A and B and S2).

In addition to well-known resident proteins of the INM/Lamina, other proteins less often associated with INM/Lamina studies were also classified in this group as potential INM/LAD links. An example would be methyl-CpG binding protein (MECP2), which we have found to interact with both LADs and in published laminome data. MECP2 is a known repressor of DNA that binds to methylated CpG regions in the DNA. Recently, a study demonstrated that CpG methylation demarcates the heterochromatic "B-compartment" of the genome, which is highly correlated with LADs (17 *Preprint*, 18 *Preprint*, 74). Consistently, bioinformatic analysis of publicly available MeCP2 ChIP-seq data shows a high coincidence of MeCP2 binding domains with LADs—with two thirds of MeCP2 occupancy coinciding with LADs and almost half of the LADs potentially regulated by MeCP2 binding events (Fig 5C–E (10, 71)). Furthermore, an interaction between LBR and MECP2, as well as HP1, has been observed, further implicating MECP2 physically interacting with the INM proteome and the LAD proteome (62, 75, 76, 77, 78, 79). Other examples in this category include TRIM28; RRP1B, which have both been documented to interact with nuclear lamina components and

shown to be associated with H3K9 methylated locations in the genome; PRR14, which has been shown to provide a link between LADs and the INM through its association with HP1; and RIF1, a known chromatin modifier involved in replication timing and previously shown to be enriched on LADs (Table 1).

Proteins associating uniquely with LADs
We found a large number of LAD-restricted proteins that did not overlap with the laminome or lap2b datasets. These proteins potentially regulate/modulate LADs independent of their association with the nuclear periphery. Proteins in this group fall under three sub-categories consisting of cell cycle regulators, proteins that bind and/or regulate DNA and proteins that bind to or modulate H3K9 methylation. We were particularly interested in the proteins that affect H3K9 methylation because the methylation of H3K9 is an important feature of heterochromatin and has been shown to be enriched at and required for LADs (10, 11, 12, 14, 15, 16, 17 *Preprint*, 18 *Preprint*, 80, 81, 82, 83). This includes the HP1 proteins, chromobox 5 (CBX5) also known as heterochromatin protein 1 α (HP1α) which binds to H3K9me3 (84) and heterochromatin protein 1 β (HP1β or CBX1). CBX1 serves a similar function as HP1α and as shown, in our bioinformatic analysis, to be highly coincident with LADs (Table 1 and Fig 6A–C (72)). We find that 80% of CBX1 binding peaks reside within LADs (Fig 6B). In addition, we detected other chromobox family proteins: chromobox 3 (CBX3 or HP1γ) and 8 (CBX8) in our BioSITe data. HP1 proteins, particularly HP1α, bind to methylated H3K9 and mediate gene silencing by maintaining and spreading heterochromatin. Alongside these HP1 proteins, we also identified
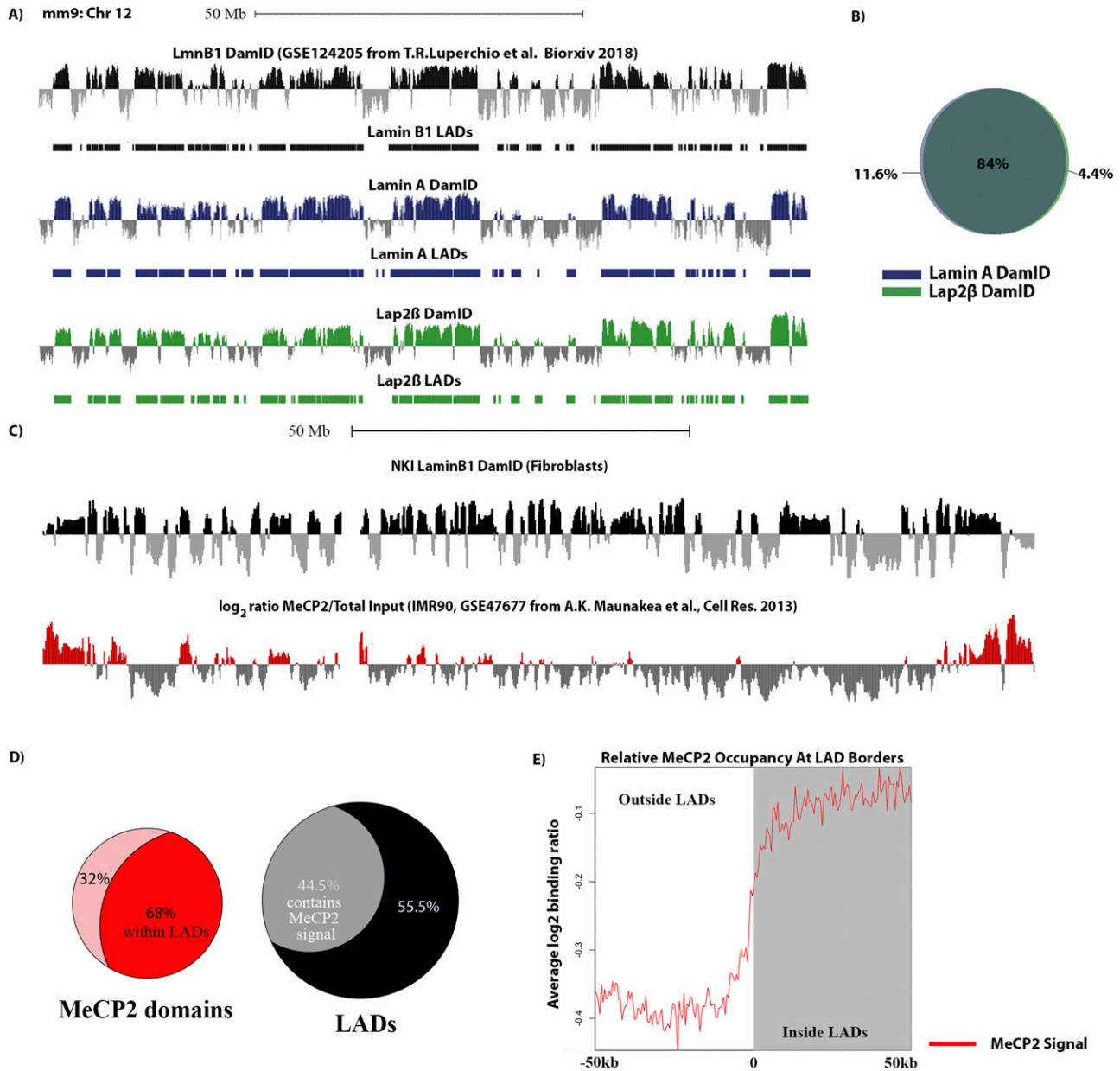
Figure 5. MeCP2 interacts with both LADs and lamin proteins (Zone2, interface between LADs and lamina). (A) Log$_2$ ratio plots from MEFs (mm9 build) chr 12 of LmnB1 DamID (black), our LaminA (blue) and Lap2β DamID (green) (17 *Preprint*). **(B)** Venn diagram showing degree of overlap in percentage between Lamin A and Lap2β lamina associated domains (LADs). **(C)** Log$_2$ ratio plots from human fibroblasts (hg19 build) chr 8 of MeCP2 occupancy (ChIP) in red, LmnB1 DamID in black (10, 70). **(D)** Venn diagrams showing the percentage (in terms of base coverage) of MeCP2 domains within LADs and the percentage (in base coverage) of LADs that are bound by MeCP2. **(E)** MeCP2 profile anchored at all boundaries of LADs of size 100 kb or greater and oriented from outside LAD (left) to inside LAD (right). Line graphs represent the average trend across all boundary profiles.

the histone chaperone and proto-oncogene DEK, which has been shown to prevent access to transcription machinery and to interact with HP1, enhancing its binding to H3K9me3 (85, 86). Furthermore we found the SUZ12 polycomb repressive complex 2 subunit (Suz12) which has been found to both stabilize HP1α and increase H3K27me3, which in turn increases the HP1$\alpha/\beta/\gamma$ binding of H3K9me3 (87).

Another intriguing protein that we identified in this group is the euchromatic lysine methyltransferase 2 (EHMT2, or often called G9a). EHMT2 is an important methyltransferase known to methylate

H3K9 and H3K27, facilitating H3K9me1 and H3K9me2 in particular, and subsequent gene silencing (88). Disruption of this protein by either epigenetic drugs or shRNA-mediated silencing disrupts peripheral heterochromatin and LAD formation (Table 1) (12, 16, 17 *Preprint*, 18 *Preprint*). Intriguingly, this protein was also recently implicated in methylating Lamin B1, an event suggested to be important for LAD organization (although, we note that we did not detect interactions of Lamin B1 and EHMT1/2 across multiple datasets) (89). Moreover, EHMT2 was found to interact with and is recruited by chromodomain Y like (CDYL), another protein we
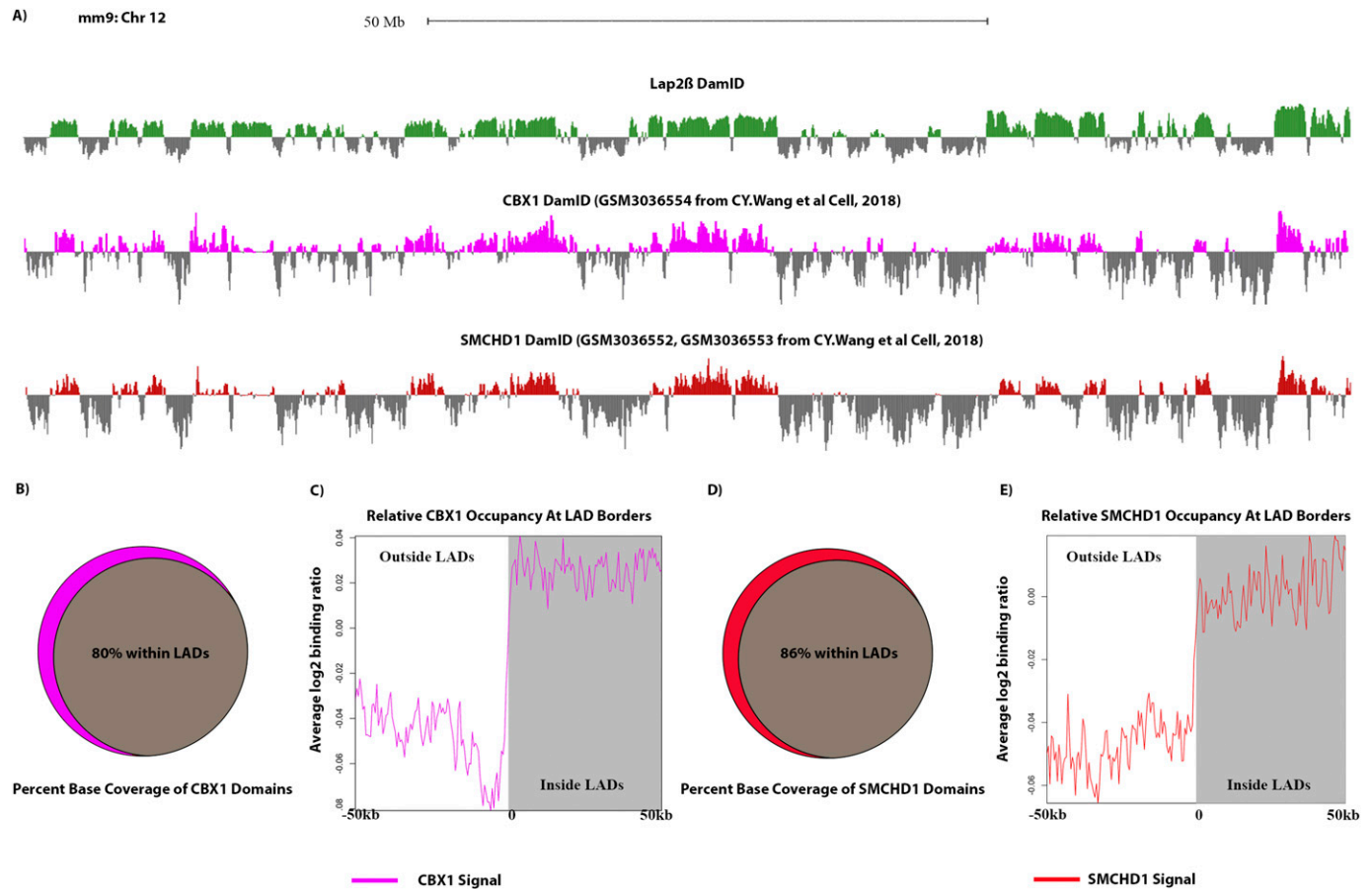
Figure 6. Both CBX1 and SMCHD1 are enriched on LADs, but do not interact with lamins (Zone 3, LAD-enriched). (A) Log₂ ratio plots from MEFs of our Lap2β DamID (green), CBX1 (also known as Hp1β, pink) and SMCHD1 DamID (Red) (71). **(B)** Venn diagram showing percentage (in base coverage) of CBX1 occupied genomic domains that overlap lamina-associated domains (LADs). **(C)** CBX1 profile anchored at all boundaries of LADs of size 100 kb or greater and oriented from outside LAD (left) to inside LAD (right). Line graphs represent the average trend across all boundary profiles for each feature. **(D)** Venn diagram showing the percentage (in base coverage) of SMCHD1 occupied genomic domains that overlap LADs. **(E)** SMCHD1 profile anchored at all boundaries of LADs of size 100 kb or greater and oriented from outside LAD (left) to inside LAD (right). Line graphs represent the average trend across all boundary profiles for each feature.

identified to be enriched at LADs, to facilitate H3K9 dimethylation and repression of the neurogenesis master regulator, REST, target genes (90, 91). EHMT2 and EHMT1 have been found to form a complex with widely interspaced zinc finger motifs (WIZ), another protein we found in our data, which acts to stabilize this complex on chromatin and prevent degradation of EHMT1 (92, 93).

Interestingly, we also identified structural maintenance of chromosomes flexible hinge domain containing 1 (SMCHD1) protein as LAD enriched—a protein that had not been previously identified on LADs. On inactive X chromosomes, SMCHD1 and HP1 are found to colocalize at areas of H3K9 methylation (72, 94 *Preprint*, 95). SMCHD1 has also been shown, by co-immunoprecipitation, to interact with ligand dependent nuclear receptor interacting factor 1 (LRIF1), another protein identified in this study, which helps target the protein to H3K9me3 regions (96). To test whether SMCHD1 interacts with LADs, as indicated by our proteomic data, we compared published SMCHD1 DamID data (from a study focused on the structural regulation of the inactive X chromosome and not LADs) with our Lap2β DamID data. This analysis showed a remarkably high coincidence rate of 86%, of SMCHD1 binding domains with LADs

suggesting that SMCHD1 potentially regulates LADs on top of its known regulatory roles in establishing and/or maintaining the inactive X chromosome (Fig 6A, D, and E (72)).

Discussion

We sought to identify the microproteome zones or regions at the INM/lamina/chromatin interface to identify potential mediators of LAD organization by mapping the LAD-proteome and comparing that to new and existing lamina/INM proteome datasets (Fig 1). Previous studies have shown that both chromatin state of the LADs and Lamin A/C are critical for LAD organization, suggesting the potential for chromatin scaffolding protein "middlemen" in mediating interactions between LADs and the lamina (97). In support of this idea, PRR14, a protein that interacts with HP1α (heterochromatin protein 1 α), has been shown to interact with both the lamina and chromatin (64, 98). Previous studies have identified proteins enriched at the nuclear lamina (the "laminome") through multiple methods, including BioID (23, 24, 25, 26, 27). Here we use BioID with BioSITe (BioID coupled with biotinylation site enrichment and

analysis) to measure proteins proximal to the INM protein Lap2β (Fig 2) in MEFs and integrate these with the previous laminome findings to generate an enhanced INM/lamina proteome map (23, 24, 25, 29, 30 Preprint, 40, 41).

Not surprisingly, most Lap2β vicinal proteins uncovered in this study were previously identified as part of the laminome. With few exceptions, most proteins unique to Lap2β interactions are other transmembrane proteins, many of which have identified roles at the plasma or cytoplasmic membranes, likely reflecting transient interactions as Lap2β transits the ER/Golgi. Exceptions to this include HMGN1, a minor groove AT-hook DNA-binding protein, and Nesprin-1 (SYNE-1), a LINC-complex protein linking the cytoskeleton to the nuclear lamina network.

To find LAD-enriched proteins, we used our BioID with BioSITe pipeline coupled with Lamin B1–directed DamID. We leveraged a modified version of a live cell LAD visualization system to recruit biotin ligase directly to LAD chromatin (Fig 1B–D). As with the Lap2β-directed BioID experiments, we verified that the biotin ligase marked proteins at the periphery of the nucleus (Figs 1B and S1). LAD-enriched proteins included cell cycle related proteins, proteins of the INM/lamina and chromatin interactors and modifiers (Fig 3B and C). Strikingly, most of the proteins identified in the LADome were specifically LAD-enriched, that is to say, they were not identified in either previous lamin interactome data or in our Lap2β interacting protein set. Importantly, LADs did not generally interact with NUPs, which is in agreement with cytological data and DamID data showing that NUPs interact primarily with transcriptionally active regions of the genome (99). NUP98, out of all the NUPs identified in the laminome, is the only NUP that displayed LAD interactions. We speculate that NUP98 interacts with LAD border regions given that it has been shown to interact with highly transcribed genes including the highly active genes that flank LADs, demarcating their borders (10).

The LAD-specific interactions highlight that although LADs and the INM/Lamina are spatially proximal, they are indeed different, but overlapping, microenvironments (Figs 3 and 7). It is especially intriguing that a large fraction of the proteins that are identified as LAD-specific are related to modulating chromatin state, particularly H3K9me2/3. Recent data from our laboratory have shown that, through the cell cycle, LADs within a chromosome self-interact before their organization at the nuclear lamina, suggesting that the higher order interactions of these chromatin domains are independent of their lamina association (17 Preprint). However, the inactive chromatin state, particularly H3K9me2/3 and H3K27me3 are required for lamina association (12, 13, 14, 15). These data are compatible with a two-step model in which chromatin state mediates self-association of these domains and that lamina association is then mediated by proteins which interact with (and help maintain) these specific chromatin modifications or states.

Of particular interest, then, are the proteins that sit at the interface of the INM/lamina and LADs. LADs were initially identified as domains of chromatin in molecular proximity to Lamin B1, using the proximity labeling method DamID. These "middlemen" proteins include Lamin A/C, emerin, and LBR, which have been previously shown to be necessary for LAD organization. In this and other studies, Lamin A/C and emerin have also been used to identify LADs, thus their identification in our screen as overlapping LADs and the INM/lamina is not surprising (65, 100, 101) (Figs 3C and 7,
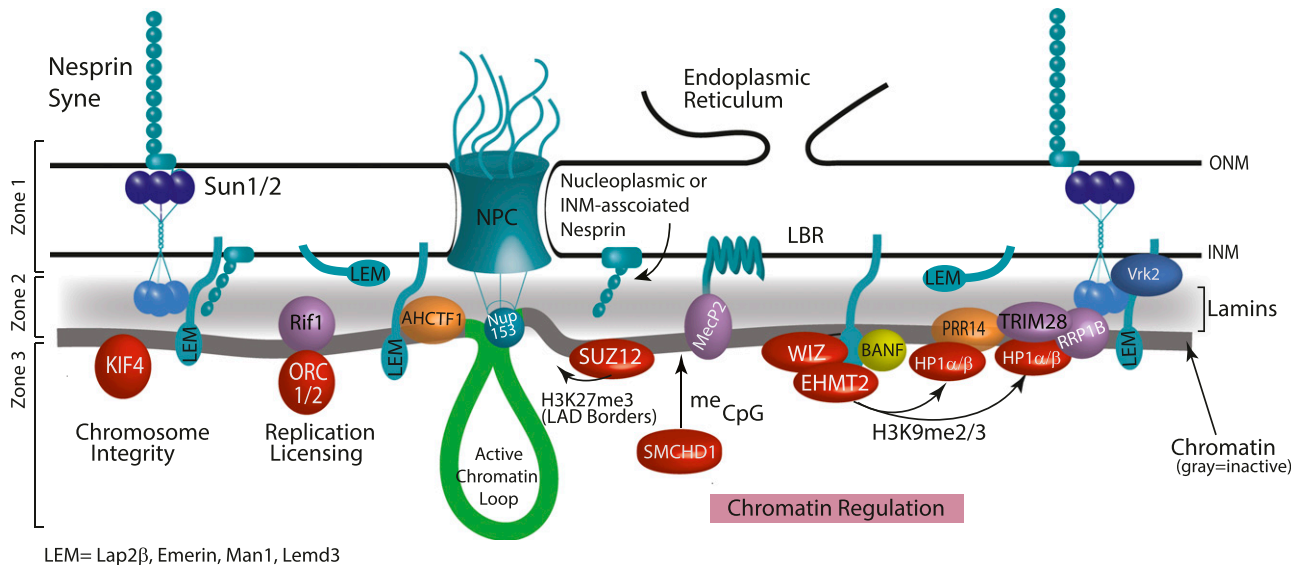

Figure 7. Putative model of the local proteome at the inner nuclear membrane (INM)/lamina/lamina-associated domain (LAD) interface.
The model depicts the nuclear periphery resolved into three zones based on data from this work as well as previous studies. Zone 1 is the most distal from chromatin comprising proteins that do not interact with LADs, such as nuclear pore complexes, some nesprins, and regulators of LEM domain proteins. Zone 1 then transitions into Zone 2 consisting of lamin proteins (shaded gray) and membrane-spanning proteins (colored teal) that traverse the lamina/LAD interface. In this region, we also find a unique set of chromatin/DNA binding proteins that display interactions with both the INM/lamina network and LADs (purple and gold). BANF, although not found in our datasets, is included in this zone based upon numerous in vivo and in vitro studies demonstrating its position as a linker between chromatin and the nuclear envelope. Thus, Zone 2 is made up of a lamin scaffold, some INM proteins, and a specific subset of DNA interacting proteins that may facilitate LAD interactions with the nuclear lamina. Finally, Zone 3 shows LAD-specific proteins (red) identified in our screen. These are highly enriched in chromatin-binding and modifying proteins.

zone 2). These "middlemen" proteins are all potential mediators of LAD organization at the lamina (12, 17 Preprint, 18 Preprint, 19). Thus, our analysis has identified known mediators of LAD scaffolding as proximally interacting with LADs.

Importantly, our BioSITe analysis also uncovered additional proteins that sit at this interface and are, heretofore, untested potential mediators of LAD organization to the nuclear lamina (Figs 3C and 7 zone 2). These include the previously implicated PRR14, as well as RIF1, AHCFT1, and MECP2 and H2AFX. RIF1 binding, which demarcates late replicating domains, has previously been identified as overlapping with LADs and in regulating genome organization (52). AHCFT1 (also known as ELYS) is implicated in nucleopore complex assembly, proper exit from mitosis, and genome stability (53, 54). MECP2, a methyl CpG binding protein, has clear roles in establishing and maintaining heterochromatin. MeCP2 partners with HDACs and histone methyl-transferase (as well as RNA) and is involved in higher order chromatin remodeling and silencing (55, 102, 103, 104, 105, 106, 107, 108, 109, 110, 111). We have also shown bioinformatically using published MeCP2 ChIP datasets that MeCP2 is enriched within LADs (Fig 5). Intriguingly, although our proteomic analysis was not suited to identifying chromatin modifications, we identified histone H2AFX, which is phosphorylated to form γH2Ax. γH2AX is found on double strand breaks on chromatin, which become heterochromatinized and possibly shunted to the nuclear periphery (112). H2Ax may also be key in establishing de novo LAD organization because one study found that during epithelial to mesenchymal transition, regions that demarcate newly formed LAD borders become enriched in γH2AX (113).

The synthesis of these data allows us to better refine a putative model of the micro-proteome of the INM/lamina and LAD interface into "zones" of interaction (Fig 7). Whereas our model in Fig 7 depicts an INM/lamina separated into three "zones" of interaction (from a LAD point-of-view), more refined and future studies will likely uncover further subdivision of the NE into additional spatio-temporal regions, perhaps enriched with specific INM proteins, with the potential to differentially regulate chromatin and other nuclear processes. Taken together, our findings suggest that LADs and the INM/Lamina have distinct, but overlapping proteomes. Several of the proteins that are shared between LADs and the INM/lamina have already been shown to be important for organization of LADs to the lamina. We propose that several newly identified proteins spanning these two proteomic domains are likely involved in establishment or maintenance of LAD chromatin. Moreover, our findings are consistent with LADs themselves, supporting a heterochromatic architecture that is independent of their association with the nuclear lamina, but important for mediating interactions at the lamina.

Materials and Methods

Plasmid construction

To clone Fu CMV DD-Dam-LMNB1, Dam LmnB1 was first amplified from Plgw Dam LmnB, kindly provided by the Van Steensel laboratory, with overhanging restriction sites. The amplicon was then TA cloned into pGEM-t easy (promega). The cdt1 fucci tag, flanked by AgeI and XmaI sites, was amplified from cDNA library of HEK293 cells. This tag was cloned into the AgeI site that lies between Dam and LmnB1. The Deadbox domain was synthesized using overlapping oligonucleotides and cloned upstream of Dam. The entire DD-Dam-hCdt1-LmnB1 fragment was then subcloned into the EcoRI and BstBI site on Fu_GFP_hLMNA Puro (unpublished).

To generate Fu-BirA-mCherry-m6A, the m6A was synthesized using codon-optimized, overlapping oligonucleotides that span the last 109 amino acids of the restriction endonuclease DpnI and amplified to be flanked by BsrGI and BstBI restriction sites. The amplicon was then cloned downstream of mCherry in the Fu-mCherry-hLMNA-bsr vector (unpublished) using BsrGI and BstBI, generating Fu-mCherry-m6a. Generation one BirA* flanked by NheI and XbaI was amplified from mycBioID-pBABE-puro, a gift from Kyle Roux, and cloned into the NheI site upstream of mCherry in Fu-mCherry-m6a.

To generate Fu-BirA* Lap2β, Lap2β was amplified from cDNA material from MEFs and TA cloned into pGEM-t easy (promega). Lap2β along with a linker sequence corresponding to the multiple cloning site of pCDNA3.1 was subcloned downstream of BirA* in Fu_BirA*_hLMNA using the XhoI and BstBI restriction sites.

Cell line generation, reagents, and antibodies

MEFs were purchased from ATCC (CRL-2752) and cultured according to their establish protocols. These MEFs were transduced with lentiviral particles from the described plasmids. Specifically, viruses were generated in HEK 293T/17 cells (CRL-11268; ATCC) by co-transfecting VSV-G, delta 8.9, and the indicated construct. 10 mM sodium butyrate was then added to the transfected cells 3 h post transfection for an overnight (~16 h) incubation at 37°C, 5% CO_2. The transfection media containing sodium butyrate was removed the following day and the cells were washed with 1× PBS. Opti-MEM was then added back to the cells which were then incubated at 37°C, 5% CO_2. Viral supernatant was collected every 12 h (up to four collections), and the supernatant of all collections were pooled. MEFs were incubated overnight with fresh viral supernatants supplemented with 4 μg/ml polybrene and 10% FBS. Fresh MEF medium was then added to the cells after the virus was removed and selected with 10 μg/ml blasticidin or 1 μg/ml puromycin (or both). Antibodies used in this study include an anti-LMNB antibody (sc-6217, goat IgG; Santa Cruz Biotechnology, Inc.), Alexa Fluor 647 AffiniPure Donkey Anti-Goat (#705-606-147; Jackson Immuno-research), and anti-biotin antibody (A150-109A; Bethyl Laboratories, Inc.).

Imaging and immunofluorescence

Cells were prepared for immunofluorescence by plating on sterilized 25-mm round coverslips (German borosilicate glass #1.5; Harvard Apparatus) in six-well tissue culture dishes. Immunofluorescence was carried out as previously described (12, 114). The nuclear lamina was visualized using an anti-LMNB antibody (sc-6217, goat IgG; Santa Cruz Biotechnology, Inc.) and Alexa Fluor 647 AffiniPure Donkey Anti-Goat (#705-606-147; Jackson Immuno-research) for secondary detection. Biotinylation was detected using streptavidin-488 (#016-540-084, Alexa Fluor 488 Streptavidin; Jackson Immunoresearch). Immunofluorescence samples were mounted in SlowFade gold (Life Technologies). All imaging was performed on an

inverted fluorescence microscope (AxioVision; Carl Zeiss) fitted with an ApoTome and camera (AxioCam MRm; Carl Zeiss). The objective lens used was a 63× apochromat oil immersion (Carl Zeiss) with an NA of 1.5 (Immersol 518; Carl Zeiss). All immunofluorescence was performed at room temperature on #1.5 coverslips. AxioVision software (Carl Zeiss) was used for image acquisition. Images were exported as TIFFs to (FIJI ImageJ, National Institutes of Health) for further analyses (115).

BioID with BioSITe

NIH3T3 cells expressing LAP2β-BioID, BirA*-m6A-tracer alone, BirA*-m6A-tracer + DD-Dam-LMNB1 constructs were cultured overnight (~16 h) with 50 μM exogenous biotin. Cells expressing BirA*-m6A-tracer + DD-Dam-LMNB1 were cultured with 2 μM shield-1 ligand (AOBIOUS, #AOB1848) for 24 h before the addition of exogenous biotin for a total of 48 h. Cells were trypsinized, washed in large volume PBS washes, then resuspended in a hypotonic lysis buffer (5 mM PIPES, 85 mM KCL, 1% NP-40, and protease inhibitors) for 10 min to separate cytoplasmic fraction from nuclear fraction. The resulting nuclei were pelleted and protein extraction was carried out by sonication (three rounds, duty cycle 30%, 20 s pulses) in 50 mM TEABC and 8 M urea. The protein concentration of samples was measured by BCA assay. A total of 10 mg of lysate per replicate was then reduced and alkylated by incubation with 10 mM DTT for 30 min followed by 20 mM IAA for 30 min in the dark. The lysate was diluted to 2 M urea by adding three cell lysate volumes of 50 mM TEABC. The proteins were digested with trypsin (1:20 of trypsin to protein) at 37°C overnight (~16 h). The resulting tryptic peptides were desalted using a Sep-PAK C18 column and subsequently lyophilized. Protein G agarose beads (#16-266; Millipore Sigma) were washed twice with PBS and 100 μg of anti-biotin antibody (A150-109A; Bethyl Laboratories, Inc.) were coupled to 120 μl of protein G bead slurry, overnight (~16 h) at 4°C. Antibody-coupled beads were further washed with PBS once and BioSITe capture buffer (50 mM Tris, 150 mM NaCl, and 0.5% Triton X-100) twice. Lyophilized peptides were dissolved in 1 ml of BioSITe capture buffer and pH solution was adjusted to neutral (7.0–7.5). Peptides were subsequently incubated with anti-biotin antibody-bound protein G beads for 1 h at 4°C. The bead slurry was washed three times with BioSITe capture buffer, three times with 50 ml of Tris, and two times with ultrapure water. Biotinylated peptides were eluted with four rounds of 200 μl elution buffer (80% acetonitrile and 0.2% trifluoroacetic acid in water). The eluents were dried, desalted, and concentrated using homemade C18 reversed-phase column.

Mass spectrometry

The fractionated peptides were analyzed on an Orbitrap Fusion Lumos Tribrid Mass spectrometer coupled to the Easy-nLC 1200 nanoflow liquid-chromatography system (Thermo Fisher Scientific). The peptides from each fraction were reconstituted in 20 μl of 0.1% formic acid and loaded onto an Acclaim PepMap 100 Nano-Trap Column (100 μm × 2 cm; Thermo Fisher Scientific) packed with 5-μm C18 particles at a flow rate of 4 μl per minute. Peptides were separated at 300 nl/min flow rate using a linear gradient of 7–30% solvent B (0.1% formic acid in 95% acetonitrile) over 95 min on an

EASY-Spray column (50 cm × 75 μm ID; Thermo Fisher Scientific) packed with 2 μm C18 particles, which was fitted with an EASY-Spray ion source that was operated at a voltage of 2.3 kV.

Mass-spectrometry analysis was carried out in a data-dependent manner with a full scan in the mass-to-charge ratio (m/z) range of 300–18,000 in the "Top Speed" setting, 3 s per cycle. MS and MS/MS were acquired for the precursor ion detection and peptide fragmentation ion detection, respectively. MS scans were measured at a resolution of 120,000 (at m/z of 200). MS/MS scans were acquired by fragmenting precursor ions using the higher energy collisional dissociation (HCD) method and detected at a mass resolution of 30,000 (at m/z of 200). Automatic gain control for MS was set to 1 million ions and for MS/MS was set to 0.05 million ions. A maximum ion injection time was set to 50 ms for MS and 100 ms for MS/MS. MS data were acquired in profile mode and MS/MS data in centroid mode. Higher energy collisional dissociation was set to 32 for MS/MS. Dynamic exclusion was set to 35 s, and singly charged ions were rejected. Internal calibration was carried out using the lock mass option (m/z 445.1200025) from ambient air.

Database searching, quantification, and post-processing of MS data

Proteome Discoverer (v 2.2; Thermo Fisher Scientific) suite was used for quantitation and identification of peptides from LC–MS/MS runs. Spectrum selector was used to import spectrum from raw file. During MS/MS preprocessing, the top 10 peaks in each window of 100 m/z were selected for database search. The tandem mass spectrometry data were then searched using SEQUEST algorithm against protein databases (mouse NCBI RefSeq 73: 58039 entries) with the addition of fasta file entries for BirA*-m6A-tracer and LAP2β-BioID constructs with common contaminant proteins. The search parameters for identification of biotinylated peptides were as follows: (i) trypsin as a proteolytic enzyme (with up to three missed cleavages); (ii) peptide mass error tolerance of 10 ppm; (iii) fragment mass error tolerance of 0.02 D; and (iv) carbamido-methylation of cysteine (+57.02146 D) as a fixed modification and oxidation of methionine (+15.99492 D) and biotinylation of lysine (+226.07759 D) as variable modifications. Peptides and proteins were filtered at a 1% false-discovery rate at the peptide spectral match (PSM) level using percolator node and at the protein level using protein false-discovery rate validator node, respectively. For the MS1 level quantification of the peptides, the Minora Feature Detector, using the program's standard parameters, was used and all of the raw files from the two replicates were quantified together. Unique and razor peptides both were used for peptide quantification, whereas protein groups were considered for peptide uniqueness. Identified protein and PSM level data were exported as tabular files from Proteome Discoverer 2.2. We used an in-house Python script to compile the peptide level site information mapped to RefSeq databases. We eliminated all non-biotinylated peptides from our analysis. The summary count on the number of supported peptides, PSMs, number of biotinylation sites and quantification was then calculated at the protein level. Quantitation of replicate agreement was plotted and average values between replicates were calculated for total biotinylated protein abundance. Transmembrane domain analysis was carried out as previously described (PMID:

28156110). We obtained annotated transmembrane domains, topological domains, and subcellular localization from Uniprot. Sites of biotinylation were then compared with annotated topologies to identify the location of biotinylation with respect to lumen, nucleoplasmic, and cytoplasmic portions of proteins. For gene set enrichment analysis, gene lists were uploaded to the Web portal Enrichr (http://amp.pharm.mssm.edu/Enrichr/) (PMID: 27141961).

DamID

DamID was performed as described previously (9, 10, 12, 20, 116). Cells were transduced with murine retroviruses harboring the Dam constructs. Self-inactivating retroviral constructs pSMGV Dam-V5 (Dam-Only), pSMGV Dam-V5-Lamin A (Dam-Lamin A), and pSMGV Dam-V5- Lap2β (Dam-Lap2β) were transfected using Fugene 6 transfection reagent (E2691; Promega) into the Platinum-E packaging line (RV-101; Cell Biolabs) to generate infectious particles. These viral supernatants in DMEM complete media were used to directly infect MEF lines. Retroviral infections were carried out by incubating MEFs overnight (~16 h) with either Dam-only, Dam-LmnA, or Dam-Lap2β viral supernatant and 4 μg/ml polybrene. Cells were allowed to expand for 2–4 d then pelleted for harvest.

MEFs were collected by trypsinization and DNA was isolated using the QIAamp DNA Mini Kit (51304; QIAGEN), followed by ethanol precipitation and resuspension to 1 μg/μl in 10 mM Tris, pH 8.0. Digestion was performed overnight (~16 h) using 0.5–2.5 μg of this genomic DNA and restriction enzyme DpnI (R0176; NEB) and then heat-killed for 20 min at 80°C. Samples were cooled, then double stranded adaptors of annealed oligonucleotides (HPLC purified; IDT) AdRt (5′-CTAA-TACGACTCACTATAGGGCA GCGTGGTCGCGGCCGAGGA-3′) and AdRb (5′-TCCTCGGCCG-3′) were ligated to the DpnI digested fragments in an overnight (~16 h) reaction at 16°C using T4 DNA ligase (799009; Roche). After incubation, the ligase was heat-inactivated at 65°C for 10 min, samples were cooled, and then digested with DpnII for 1 h at 37°C (R0543; NEB). These ligated pools were then amplified using AdR_PCR oligonucleotides as primer (5′-GGTCGCGGCCGAGGATC-3′) (IDT) and Advantage cDNA polymerase mix (639105; Clontech). Amplicons were electrophoresed in 1% agarose gel to check for amplification and the size distribution of the library and then column purified (28104; QIAGEN). Once purified, material was checked for LAD enrichment via qPCR (4368577 and StepOne Plus machine; Applied Biosystems) using controls specific to an internal Immunoglobulin heavy chain (Igh) LAD region (J558 1, 5′-AGTGCAGGGCTCACAGAAAA-3′, and J558 12, 5′-CAGCTCCATCCCATGGT TAGA-3′) for validation before sequencing.

DamID-seq library preparation and sequencing

To ensure sequencing of all DamID fragments, post-DamID–amplified material was randomized by performing an end repair reaction, followed by ligation and sonication. Specifically, 0.5–5 μg of column purified DamID material (from above) was end-repaired using the NEBNext End Repair Module (E6050S; NEB) following the manufacturer's recommendations. After purification using the QIAquick PCR Purification Kit (28104; QIAGEN), 1 μg of this material was then ligated in a volume of 20 μl with 1 μl of T4 DNA ligase (10799009001; Roche) at 16°C to generate a randomized library of large

fragments. These large fragments were sonicated (in a volume of 200 μl, 10 mM Tris, pH 8.0) to generate fragments suitable for sequencing using a Bioruptor UCD-200 at high power, 30 s ON, 30 s OFF for 1 h in a 1.5 ml DNA LoBind microfuge tube (022431005; Eppendorf). The DNA was then transferred to 1.5 ml TPX tubes (C30010010-1000; Diagenode) and sonicated for four rounds of 10 min (high power, 30 s ON and 30 s OFF). The DNA was transferred to new TPX tubes after each round to prevent etching of the TPX plastic. The sonication procedure yielded DNA sizes ranging from 100 to 200 bp. After sonication, the DNA was precipitated by adding 20 μl of 3 M sodium acetate, pH 5.5 and 500 μl ethanol, supplemented with 3 μl of glycogen (molecular biology grade, 20 mg/ml), and kept at −80°C for at least 2 h. The DNA mix was centrifuged at full speed for 10 min to pellet the sheared DNA with the carrier glycogen. The pellet was washed with 70% ethanol and then centrifuged again at full speed. The DNA pellet was then left to air dry. 20 μl of 10 mM Tris–HCl was used to resuspend the DNA pellet. 1 μl was quantified using the Quant-iT PicoGreen dsDNA kit (P7589; Invitrogen). Sequencing library preparation was performed using the NEBNext Ultra DNA library prep kit for Illumina (E7370S; NEB), following the manufacturer's instructions. Library quality and size was determined using a Bioanalyzer 2100 with DNA High Sensitivity reagents (5067-4626; Agilent). Libraries were then quantified using the Kapa quantification Complete kit for Illumina (KK4824; Kapa Biosystems) on an Applied Biosystems 7500 Real Time qPCR system. Samples were normalized and pooled for multiplex sequencing.

DamID-seq data processing

DamID-seq analysis—DamID-seq reads were processed using LADetector (available at https://github.com/thereddylab/LADetector), an updated implementation of the previously described LADetector (12) with incorporated sequence mapping. Specifically, 5′ ends of reads were quality trimmed using a sliding window quality score average over three bases and a minimum score cutoff of 30. This was followed by trimming any matching overlap between read-ends and sequencing or DamID adaptor-primer sequence. Reads containing a DamID adaptor-primer sequence were split and adaptor-primer sequence removed. All resulting reads greater than 20 bp were aligned to mm9 using Bowtie (117) with parameters "—tryhard–best–m 1." Unaligned reads had 13 bases trimmed from the 5′ end and remapped, and the resultant unmapped reads were trimmed 13 bases from the 3′ end and remapped. Total aligned reads were assigned to *Dpn*I bins, with reads straddling bin boundaries counting toward both. Before scoring, a value of 0.5 was added to bins with no reads. Bins falling in unaligned regions were removed before analysis. DamID scores were calculated for all non-zero bins as the log$_2$ ratio of Dam-Lamin B1 over unfused Dam. Scores were partitioned using circular binary segmentation using the DNAcopy package in R (118, 119, 120). LADs were classified as regions >100 kb in size of positive signals, allowing for smaller regions of negative signal <10 kb in size.

Data Availability

The mass spectrometry proteomics data have been deposited to the ProteomeXchange Consortium (http://proteomecentral.proteomexchange.

Supplementary Information

Supplementary Information is available at https://doi.org/10.26508/lsa.202000774.

Acknowledgements

Author Contributions

X Wong: conceptualization, data curation, software, formal analysis, validation, investigation, visualization, methodology, and writing—review and editing.
JA Cutler: conceptualization, formal analysis, investigation, visualization, methodology, and writing—review and editing.
VE Hoskins: investigation and writing—review and editing.
M Gordon: investigation.
AK Madugundu: resources and investigation.
A Pandey: resources and supervision.
KL Reddy: conceptualization, data curation, supervision, funding acquisition, investigation, visualization, methodology, project administration, and writing—original draft, review, and editing.

Conflict of Interest Statement

The authors declare that they have no conflict of interest.

References

1. Cockell M, Gasser SM (1999) Nuclear compartments and gene regulation. *Curr Opin Genet Dev* 9: 199–205. doi:10.1016/s0959-437x(99)80030-6

2. Cremer T, Kreth G, Koester H, Fink RH, Heintzmann R, Cremer M, Solovei I, Zink D, Cremer C (2000) Chromosome territories, interchromatin domain compartment, and nuclear matrix: An integrated view of the functional nuclear architecture. *Crit Rev Eukaryot Gene Expr* 10: 179–212. doi:10.1615/critreveukargeneexpr.v10.i2.60

3. Misteli T (2007) Beyond the sequence: Cellular organization of genome function. *Cell* 128: 787–800. doi:10.1016/j.cell.2007.01.028

4. Wong X, Luperchio TR, Reddy KL (2014) NET gains and losses: The role of changing nuclear envelope proteomes in genome regulation. *Curr Opin Cell Biol* 28: 105–120. doi:10.1016/j.ceb.2014.04.005

5. Dekker J, Marti-Renom MA, Mirny LA (2013) Exploring the three-dimensional organization of genomes: Interpreting chromatin interaction data. *Nat Rev Genet* 14: 390–403. doi:10.1038/nrg3454

6. Nora EP, Dekker J, Heard E (2013) Segmental folding of chromosomes: A basis for structural and regulatory chromosomal neighborhoods? *Bioessays* 35: 818–828. doi:10.1002/bies.201300040

7. Luperchio TR, Wong X, Reddy KL (2014) Genome regulation at the peripheral zone: Lamina associated domains in development and disease. *Curr Opin Genet Dev* 25: 50–61. doi:10.1016/j.gde.2013.11.021

8. van Steensel B, Belmont AS (2017) Lamina-associated domains: Links with chromosome architecture, heterochromatin, and gene repression. *Cell* 169: 780–791. doi:10.1016/j.cell.2017.04.022

9. Vogel MJ, Peric-Hupkes D, van Steensel B (2007) Detection of in vivo protein–DNA interactions using DamID in mammalian cells. *Nat Protoc* 2: 1467–1478. doi:10.1038/nprot.2007.148

10. Guelen L, Pagie L, Brasset E, Meuleman W, Faza MB, Talhout W, Eussen BH, de Klein A, Wessels L, de Laat W, et al (2008) Domain organization of human chromosomes revealed by mapping of nuclear lamina interactions. *Nature* 453: 948–951. doi:10.1038/nature06947

11. Wen B, Wu H, Shinkai Y, Irizarry RA, Feinberg AP (2009) Large histone H3 lysine 9 dimethylated chromatin blocks distinguish differentiated from embryonic stem cells. *Nat Genet* 41: 246–250. doi:10.1038/ng.297

12. Harr JC, Luperchio TR, Wong X, Cohen E, Wheelan SJ, Reddy KL (2015) Directed targeting of chromatin to the nuclear lamina is mediated by chromatin state and A-type lamins. *J Cell Biol* 208: 33–52. doi:10.1083/jcb.201405110

13. Kind J, Pagie L, de Vries SS, Nahidiazar L, Dey SS, Bienko M, Zhan Y, Lajoie B, de Graaf CA, Amendola M, et al (2015) Genome-wide maps of nuclear lamina interactions in single human cells. *Cell* 163: 134–147. doi:10.1016/j.cell.2015.08.040

14. Bian Q, Khanna N, Alvikas J, Belmont AS (2013) β-Globin cis-elements determine differential nuclear targeting through epigenetic modifications. *J Cell Biol* 203: 767–783. doi:10.1083/jcb.201305027

15. Towbin BD, González-Aguilera C, Sack R, Gaidatzis D, Kalck V, Meister P, Askjaer P, Gasser SM (2012) Step-wise methylation of histone H3K9 positions heterochromatin at the nuclear periphery. *Cell* 150: 934–947. doi:10.1016/j.cell.2012.06.051

16. Kind J, Pagie L, Ortabozkoyun H, Boyle S, de Vries SS, Janssen H, Amendola M, Nolen LD, Bickmore WA, van Steensel B (2013) Single-cell dynamics of genome-nuclear lamina interactions. *Cell* 153: 178–192. doi:10.1016/j.cell.2013.02.028

17. Luperchio TR, Sauria MEG, Hoskins VE, Xianrong W, DeBoy E, Gaillard M-C, Tsang P, Pekrun K, Ach RA, Yamada A, et al (2018) The repressive genome compartment is established early in the cell cycle before forming the lamina associated domains. BioRxiv doi:10.1101/481598 Preprint posted November 29, 2018.

18. Luperchio TR, Sauria MEG, Wong X, Gaillard M-C, Tsang P, Pekrun K, Ach RA, Yamada NA, Taylor J, Reddy K (2017) Chromosome conformation paints reveal the role of lamina association in genome organization and regulation. BioRxiv doi:10.1101/122226 Preprint posted March 30, 2017.

19. Solovei I, Wang AS, Thanisch K, Schmidt CS, Krebs S, Zwerger M, Cohen TV, Devys D, Foisner R, Peichl L, et al (2013) LBR and lamin A/C sequentially tether peripheral heterochromatin and inversely regulate differentiation. *Cell* 152: 584–598. doi:10.1016/j.cell.2013.01.009

20. Zullo JM, Demarco IA, Piqué-Regi R, Gaffney DJ, Epstein CB, Spooner CJ, Luperchio TR, Bernstein BE, Pritchard JK, Reddy KL, et al (2012) DNA sequence-dependent compartmentalization and silencing of chromatin at the nuclear lamina. *Cell* 149: 1474–1487. doi:10.1016/j.cell.2012.04.035

21. Kim Y, Zheng X, Zheng Y (2019) Role of lamins in 3D genome organization and global gene expression. *Nucleus* 10: 33–41. doi:10.1080/19491034.2019.1578601

22. Zheng X, Hu J, Yue S, Kristiani L, Kim M, Sauria M, Taylor J, Kim Y, Zheng Y (2018) Lamins organize the global three-dimensional genome from the

nuclear periphery. *Mol Cell* 71: 802–815.e7. doi:10.1016/j.molcel.2018.05.017

23. Xie W, Chojnowski A, Boudier T, Lim JSY, Ahmed S, Ser Z, Stewart C, Burke B (2016) A-type lamins form distinct filamentous networks with differential nuclear pore complex associations. *Curr Biol* 26: 2651–2658. doi:10.1016/j.cub.2016.07.049

24. Kim DI, Jensen SC, Roux KJ (2016) Identifying protein-protein associations at the nuclear envelope with BioID. *Methods Mol Biol* 1411: 133–146. doi:10.1007/978-1-4939-3530-7_8

25. Roux KJ, Kim DI, Raida M, Burke B (2012) A promiscuous biotin ligase fusion protein identifies proximal and interacting proteins in mammalian cells. *J Cell Biol* 196: 801–810. doi:10.1083/jcb.201112098

26. Roux KJ, Kim DI, Burke B (2013) BioID: A screen for protein-protein interactions. *Curr Protoc Protein Sci* 74: 19.23.1-19.23.14. doi:10.1002/0471140864.ps1923s74

27. Mehus AA, Anderson RH, Roux KJ (2016) BioID identification of lamin-associated proteins. *Methods Enzymol* 569: 3–22. doi:10.1016/bs.mie.2015.08.008

28. Schmidtmann E, Anton T, Rombaut P, Herzog F, Leonhardt H (2016) Determination of local chromatin composition by CasID. *Nucleus* 7: 476–484. doi:10.1080/19491034.2016.1239000

29. Kim DI, Birendra KC, Zhu W, Motamedchaboki K, Doye V, Roux KJ (2014) Probing nuclear pore complex architecture with proximity-dependent biotinylation. *Proc Natl Acad Sci U S A* 111: E2453–E2461. doi:10.1073/pnas.1406459111

30. Bar DZ, Atkatsh K, Tavarez U, Erdos MR, Gruenbaum Y, Collins FS (2016) Biotinylation by antibody recognition: A novel method for proximity labeling. BioRxiv doi:10.1101/069187 Preprint posted August 11, 2016.

31. Holmer L, Worman HJ (2001) Inner nuclear membrane proteins: Functions and targeting. *Cell Mol Life Sci* 58: 1741–1747. doi:10.1007/pl00000813

32. Barton LJ, Soshnev AA, Geyer PK (2015) Networking in the nucleus: A spotlight on LEM-domain proteins. *Curr Opin Cell Biol* 34: 1–8. doi:10.1016/j.ceb.2015.03.005

33. Wong X, Hoskins VE, Harr JC, Gordon M, Reddy KL (2020) Lamin C regulates genome organization after mitosis. BioRxiv doi:10.1101/2020.07.28.213884 Preprint posted July 28, 2020.

34. Sakaue-Sawano A, Kurokawa H, Morimura T, Hanyu A, Hama H, Osawa H, Kashiwagi S, Fukami K, Miyata T, Miyoshi H, et al (2008) Visualizing spatiotemporal dynamics of multicellular cell-cycle progression. *Cell* 132: 487–498. doi:10.1016/j.cell.2007.12.033

35. Kim DI, Cutler JA, Na CH, Reckel S, Renuse S, Madugundu AK, Tahir R, Goldschmidt HL, Reddy KL, Huganir RL, et al (2018) BioSITe: A method for direct detection and quantitation of site-specific biotinylation. *J Proteome Res* 17: 759–769. doi:10.1021/acs.jproteome.7b00775

36. Chojnowski A, Sobota RM, Ong PF, Xie W, Wong X, Dreesen O, Burke B, Stewart CL (2018) 2C-BioID: An advanced two component BioID system for precision mapping of protein interactomes. *iScience* 10: 40–52. doi:10.1016/j.isci.2018.11.023

37. Volkova EG, Abramchuk SS, Sheval EV (2012) The overexpression of nuclear envelope protein Lap2β induces endoplasmic reticulum reorganisation via membrane stacking. *Biol Open* 1: 802–805. doi:10.1242/bio.20121537

38. Gaillard M-C, Reddy KL (2018) The nuclear lamina and genome organization. In Nuclear Architecture and Dynamics. Lavelle C, Victor J-M (eds.). pp 321–343. Boston: Academic Press.

39. Chen EY, Tan CM, Kou Y, Duan Q, Wang Z, Meirelles GV, Clark NR, Ma'ayan A (2013) Enrichr: Interactive and collaborative HTML5 gene list enrichment analysis tool. *BMC Bioinformatics* 14: 128. doi:10.1186/1471-2105-14-128

40. Kim DI, Birendra K, Roux KJ (2015) Making the LINC: SUN and KASH protein interactions. *Biol Chem* 396: 295–310. doi:10.1515/hsz-2014-0267

41. Birendra KC, May DG, Benson BV, Kim DI, Shivega WG, Ali MH, Faustino RS, Campos AR, Roux KJ (2017) VRK2A is an A-type lamin–dependent nuclear envelope kinase that phosphorylates BAF. *Mol Biol Cell* 28: 2241–2250. doi:10.1091/mbc.E17-03-0138

42. Furukawa K (1999) LAP2 binding protein 1 (L2BP1/BAF) is a candidate mediator of LAP2-chromatin interaction. *J Cell Sci* 112: 2485–2492.

43. Gotzmann J, Foisner R (1999) Lamins and lamin-binding proteins in functional chromatin organization. *Crit Rev Eukaryot Gene Expr* 9: 257–265. doi:10.1615/critreveukargeneexpr.v9.i3-4.100

44. Somech R, Shaklai S, Geller O, Amariglio N, Simon AJ, Rechavi G, Gal-Yam EN (2005) The nuclear-envelope protein and transcriptional repressor LAP2beta interacts with HDAC3 at the nuclear periphery, and induces histone H4 deacetylation. *J Cell Sci* 118: 4017–4025. doi:10.1242/jcs.02521

45. Kavanagh DM, Powell WE, Malik P, Lazou V, Schirmer EC (2007) Organelle proteome variation among different cell types: Lessons from nuclear membrane proteins. *Subcell Biochem* 43: 51–76. doi:10.1007/978-1-4020-5943-8_5

46. Zielke N, Edgar BA (2015) FUCCI sensors: Powerful new tools for analysis of cell proliferation. *Wiley Interdiscip Rev Dev Biol* 4: 469–487. doi:10.1002/wdev.189

47. Nishitani H, Sugimoto N, Roukos V, Nakanishi Y, Saijo M, Obuse C, Tsurimoto T, Nakayama KI, Nakayama K, Fujita M, et al (2006) Two E3 ubiquitin ligases, SCF-Skp2 and DDB1-Cul4, target human Cdt1 for proteolysis. *EMBO J* 25: 1126–1136. doi:10.1038/sj.emboj.7601002

48. Sugiyama M, Sakaue-Sawano A, Iimura T, Fukami K, Kitaguchi T, Kawakami K, Okamoto H, Higashijima S-I, Miyawaki A (2009) Illuminating cell-cycle progression in the developing zebrafish embryo. *Proc Natl Acad Sci U S A* 106: 20812–20817. doi:10.1073/pnas.0906464106

49. Banaszynski LA, Chen L-C, Maynard-Smith LA, Ooi AGL, Wandless TJ (2006) A rapid, reversible, and tunable method to regulate protein function in living cells using synthetic small molecules. *Cell* 126: 995–1004. doi:10.1016/j.cell.2006.07.025

50. Maynard-Smith LA, Chen L-C, Banaszynski LA, Ooi AGL, Wandless TJ (2007) A directed approach for engineering conditional protein stability using biologically silent small molecules. *J Biol Chem* 282: 24866–24872. doi:10.1074/jbc.m703902200

51. Cornacchia D, Dileep V, Quivy J, Foti R, Tili F, Santarella-Mellwig R, Antony C, Almouzni G, Gilbert DM, Buonomo SBC (2012) Mouse Rif1 is a key regulator of the replication-timing programme in mammalian cells. *EMBO J* 31: 3678–3690. doi:10.1038/emboj.2012.214

52. Foti R, Gnan S, Cornacchia D, Dileep V, Bulut-Karslioglu A, Diehl S, Buness A, Klein FA, Huber W, Johnstone E, et al (2016) Nuclear architecture organized by Rif1 underpins the replication-timing program. *Mol Cell* 61: 260–273. doi:10.1016/j.molcel.2015.12.001

53. Rasala BA, Orjalo AV, Shen Z, Briggs S, Forbes DJ (2006) ELYS is a dual nucleoporin/kinetochore protein required for nuclear pore assembly and proper cell division. *Proc Natl Acad Sci U S A* 103: 17801–17806. doi:10.1073/pnas.0608484103

54. Gao N, Davuluri G, Gong W, Seiler C, Lorent K, Furth EE, Kaestner KH, Pack M (2011) The nuclear pore complex protein Elys is required for genome stability in mouse intestinal epithelial progenitor cells. *Gastroenterology* 140: 1547–1555.e10. doi:10.1053/j.gastro.2011.01.048

55. Nikitina T, Shi X, Ghosh RP, Horowitz-Scherer RA, Hansen JC, Woodcock CL (2007) Multiple modes of interaction between the methylated DNA binding protein MeCP2 and chromatin. *Mol Cell Biol* 27: 864–877. doi:10.1128/mcb.01593-06

56. Jenuwein T, Laible G, Dorn R, Reuter G (1998) SET domain proteins modulate chromatin domains in eu- and heterochromatin. *Cell Mol Life Sci* 54: 80–93. doi:10.1007/s000180050127

57. Cuddapah S, Schones DE, Cui K, Roh T-Y, Barski A, Wei G, Rochman M, Bustin M, Zhao K (2011) Genomic profiling of HMGN1 reveals an association with chromatin at regulatory regions. *Mol Cell Biol* 31: 700–709. doi:10.1128/mcb.00740-10

58. Postnikov Y, Bustin M (2010) Regulation of chromatin structure and function by HMGN proteins. *Biochim Biophys Acta* 1799: 62–68. doi:10.1016/j.bbagrm.2009.11.016

59. Zhang Q, Ragnauth CD, Skepper JN, Worth NF, Warren DT, Roberts RG, Weissberg PL, Ellis JA, Shanahan CM (2005) Nesprin-2 is a multi-isomeric protein that binds lamin and emerin at the nuclear envelope and forms a subcellular network in skeletal muscle. *J Cell Sci* 118: 673–687. doi:10.1242/jcs.01642

60. Rajgor D, Mellad JA, Autore F, Zhang Q, Shanahan CM (2012) Multiple novel nesprin-1 and nesprin-2 variants act as versatile tissue-specific intracellular scaffolds. *PLoS One* 7: e40098. doi:10.1371/journal.pone.0040098

61. Ibarra A, Benner C, Tyagi S, Cool J, Hetzer MW (2016) Nucleoporin-mediated regulation of cell identity genes. *Genes Dev* 30: 2253–2258. doi:10.1101/gad.287417.116

62. Guarda A, Bolognese F, Bonapace IM, Badaracco G (2009) Interaction between the inner nuclear membrane lamin B receptor and the heterochromatic methyl binding protein, MeCP2. *Exp Cell Res* 315: 1895–1903. doi:10.1016/j.yexcr.2009.01.019

63. Rual J-F, Venkatesan K, Hao T, Hirozane-Kishikawa T, Dricot A, Li N, Berriz GF, Gibbons FD, Dreze M, Ayivi-Guedehoussou N, et al (2005) Towards a proteome-scale map of the human protein-protein interaction network. *Nature* 437: 1173–1178. doi:10.1038/nature04209

64. Poleshko A, Mansfield KM, Burlingame CC, Andrake MD, Shah NR, Katz RA (2013) The human protein PRR14 tethers heterochromatin to the nuclear lamina during interphase and mitotic exit. *Cell Rep* 5: 292–301. doi:10.1016/j.celrep.2013.09.024

65. Kind J, van Steensel B (2014) Stochastic genome-nuclear lamina interactions: Modulating roles of lamin A and BAF. *Nucleus* 5: 124–130. doi:10.4161/nucl.28825

66. Lee M, Dworkin AM, Lichtenberg J, Patel SJ, Trivedi NS, Gildea D, Bodine DM, Crawford NPS (2014) Metastasis-associated protein ribosomal RNA processing 1 homolog B (RRP1B) modulates metastasis through regulation of histone methylation. *Mol Cancer Res* 12: 1818–1828. doi:10.1158/1541-7786.mcr-14-0167

67. Kubben N, Voncken JW, Demmers J, Calis C, van Almen G, Pinto Y, Misteli T (2010) Identification of differential protein interactors of lamin A and progerin. *Nucleus* 1: 513–525. doi:10.4161/nucl.1.6.13512

68. Jang SM, Kauzlaric A, Quivy J-P, Pontis J, Rauwel B, Coluccio A, Offner S, Duc J, Turelli P, Almouzni G, et al (2018) KAP1 facilitates reinstatement of heterochromatin after DNA replication. *Nucleic Acids Res* 46: 8788–8802. doi:10.1093/nar/gky580

69. Ayyanathan K, Lechner MS, Bell P, Maul GG, Schultz DC, Yamada Y, Tanaka K, Torigoe K, Rauscher FJ 3rd (2003) Regulated recruitment of HP1 to a euchromatic gene induces mitotically heritable, epigenetic gene silencing: A mammalian cell culture model of gene variegation. *Genes Dev* 17: 1855–1869. doi:10.1101/gad.1102803

70. Alsarraj J, Faraji F, Geiger TR, Mattaini KR, Williams M, Wu J, Ha N-H, Merlino T, Walker RC, Bosley AD, et al (2013) BRD4 short isoform interacts with RRP1B, SIPA1 and components of the LINC complex at the inner face of the nuclear membrane. *PLoS One* 8: e80746. doi:10.1371/journal.pone.0080746

71. Maunakea AK, Chepelev I, Cui K, Zhao K (2013) Intragenic DNA methylation modulates alternative splicing by recruiting MeCP2 to promote exon recognition. *Cell Res* 23: 1256–1269. doi:10.1038/cr.2013.110

72. Wang C-Y, Jégu T, Chu H-P, Oh HJ, Lee JT (2018) SMCHD1 merges chromosome compartments and assists formation of super-structures on the inactive X. *Cell* 174: 406–421.e25. doi:10.1016/j.cell.2018.05.007

73. Nozawa R-S, Nagao K, Masuda H-T, Iwasaki O, Hirota T, Nozaki N, Kimura H, Obuse C (2010) Human POGZ modulates dissociation of HP1alpha from mitotic chromosome arms through Aurora B activation. *Nat Cell Biol* 12: 719–727. doi:10.1038/ncb2075

74. Fortin J-P, Hansen KD (2015) Reconstructing A/B compartments as revealed by Hi-C using long-range correlations in epigenetic data. *Genome Biol* 16: 180. doi:10.1186/s13059-015-0741-y

75. Goldberg M, Harel A, Gruenbaum Y (1999) The nuclear lamina: Molecular organization and interaction with chromatin. *Crit Rev Eukaryot Gene Expr* 9: 285–293. doi:10.1615/critreveukargeneexpr.v9.i3-4.130

76. Polioudaki H, Kourmouli N, Drosou V, Bakou A, Theodoropoulos PA, Singh PB, Giannakouros T, Georgatos SD (2001) Histones H3/H4 form a tight complex with the inner nuclear membrane protein LBR and heterochromatin protein 1. *EMBO Rep* 2: 920–925. doi:10.1093/embo-reports/kve199

77. Lechner MS, Schultz DC, Negorev D, Maul GG, Rauscher FJ 3rd (2005) The mammalian heterochromatin protein 1 binds diverse nuclear proteins through a common motif that targets the chromoshadow domain. *Biochem Biophys Res Commun* 331: 929–937. doi:10.1016/j.bbrc.2005.04.016

78. Gant TM, Wilson KL (1997) Nuclear assembly. *Annu Rev Cell Dev Biol* 13: 669–695. doi:10.1146/annurev.cellbio.13.1.669

79. Kourmouli N, Theodoropoulos PA, Dialynas G, Bakou A, Politou AS, Cowell IG, Singh PB, Georgatos SD (2000) Dynamic associations of heterochromatin protein 1 with the nuclear envelope. *EMBO J* 19: 6558–6568. doi:10.1093/emboj/19.23.6558

80. Harr JC, Gonzalez-Sandoval A, Gasser SM (2016) Histones and histone modifications in perinuclear chromatin anchoring: From yeast to man. *EMBO Rep* 17: 139–155. doi:10.15252/embr.201541809

81. Czapiewski R, Robson MI, Schirmer EC (2016) Anchoring a leviathan: How the nuclear membrane tethers the genome. *Front Genet* 7: 82. doi:10.3389/fgene.2016.00082

82. Kim J, Kim H (2012) Recruitment and biological consequences of histone modification of H3K27me3 and H3K9me3. *ILAR J* 53: 232–239. doi:10.1093/ilar.53.3-4.232

83. Saksouk N, Simboeck E, Déjardin J (2015) Constitutive heterochromatin formation and transcription in mammals. *Epigenetics Chromatin* 8: 3. doi:10.1186/1756-8935-8-3

84. Maison C, Almouzni G (2004) HP1 and the dynamics of heterochromatin maintenance. *Nat Rev Mol Cell Biol* 5: 296–304. doi:10.1038/nrm1355

85. Kappes F, Waldmann T, Mathew V, Yu J (2011) The DEK oncoprotein is a Su (var) that is essential to heterochromatin integrity. *Genes Dev* 25: 673–678. doi:10.1101/gad.2036411

86. Gamble MJ, Fisher RP (2007) SET and PARP1 remove DEK from chromatin to permit access by the transcription machinery. *Nat Struct Mol Biol* 14: 548–555. doi:10.1038/nsmb1248

87. Boros J, Arnoult N, Stroobant V, Collet J-F, Decottignies A (2014) Polycomb repressive complex 2 and H3K27me3 cooperate with H3K9 methylation to maintain heterochromatin protein 1α at chromatin. *Mol Cell Biol* 34: 3662–3674. doi:10.1128/mcb.00205-14

88. Shinkai Y, Tachibana M (2011) H3K9 methyltransferase G9a and the related molecule GLP. *Genes Dev* 25: 781–788. doi:10.1101/gad.2027411

89. Rao RA, Ketkar AA, Kedia N, Krishnamoorthy VK, Lakshmanan V, Kumar P, Mohanty A, Kumar SD, Raja SO, Gulyani A, et al (2019) KMT1 family methyltransferases regulate heterochromatin–nuclear periphery tethering via histone and non-histone protein methylation. *EMBO Rep* 20: e43260. doi:10.15252/embr.201643260

90. Mulligan P, Westbrook TF, Ottinger M, Pavlova N, Chang B, Macia E, Shi Y-J, Barretina J, Liu J, Howley PM, et al (2008) CDYL bridges REST and histone methyltransferases for gene repression and suppression of cellular transformation. *Mol Cell* 32: 718–726. doi:10.1016/j.molcel.2008.10.025

91. Escamilla-Del-Arenal M, da Rocha ST, Spruijt CG, Masui O, Renaud O, Smits AH, Margueron R, Vermeulen M, Heard E (2013) Cdyl, a new partner of the inactive X chromosome and potential reader of

H3K27me3 and H3K9me2. *Mol Cell Biol* 33: 5005–5020. doi:10.1128/mcb.00866-13

92. Bian C, Chen Q, Yu X (2015) Correction: The zinc finger proteins ZNF644 and WIZ regulate the G9a/GLP complex for gene repression. *Elife* 4: e08168. doi:10.7554/elife.08168

93. Ueda J, Tachibana M, Ikura T, Shinkai Y (2006) Zinc finger protein Wiz links G9a/GLP histone methyltransferases to the co-repressor molecule CtBP. *J Biol Chem* 281: 20120–20128. doi:10.1074/jbc.m603087200

94. Jansz N, Keniry A, Trussart M, Bildsoe H, Beck T (2018) Long-range chromatin interactions on the inactive X and at Hox clusters are regulated by the non-canonical SMC protein Smchd1. BioRxiv doi:10.1101/342212 Preprint posted June 08, 2018.

95. Nozawa R-S, Nagao K, Igami K-T, Shibata S, Shirai N, Nozaki N, Sado T, Kimura H, Obuse C (2013) Human inactive X chromosome is compacted through a PRC2-independent SMCHD1-HBiX1 pathway. *Nat Struct Mol Biol* 20: 566–573. doi:10.1038/nsmb.2532

96. Brideau NJ, Coker H, Gendrel A-V, Alistair Siebert C, Bezstarosti K, Demmers J, Poot RA, Nesterova TB, Brockdorff N (2015) Independent mechanisms target SMCHD1 to trimethylated histone H3 lysine 9-modified chromatin and the inactive X chromosome. *Mol Cell Biol* 35: 4053–4068. doi:10.1128/mcb.00432-15

97. Wong X, Reddy KL (2015) Finding the middlemen in genome organization. *Dev Cell* 35: 670–671. doi:10.1016/j.devcel.2015.12.007

98. Poleshko A, Katz RA (2014) Specifying peripheral heterochromatin during nuclear lamina reassembly. *Nucleus* 5: 32–39. doi:10.4161/nucl.28167

99. Kalverda B, Pickersgill H, Shloma VV, Fornerod M (2010) Nucleoporins directly stimulate expression of developmental and cell-cycle genes inside the nucleoplasm. *Cell* 140: 360–371. doi:10.1016/j.cell.2010.01.011

100. Robson MI, Schirmer EC (2016) The application of DamID to identify peripheral gene sequences in differentiated and primary cells. *Methods Mol Biol* 1411: 359–386. doi:10.1007/978-1-4939-3530-7_23

101. Amendola M, van Steensel B (2015) Nuclear lamins are not required for lamina-associated domain organization in mouse embryonic stem cells. *EMBO Rep* 16: 610–617. doi:10.15252/embr.201439789

102. Jones PL, Veenstra GJ, Wade PA, Vermaak D, Kass SU, Landsberger N, Strouboulis J, Wolffe AP (1998) Methylated DNA and MeCP2 recruit histone deacetylase to repress transcription. *Nat Genet* 19: 187–191. doi:10.1038/561

103. Dhasarathy A, Wade PA (2008) The MBD protein family-reading an epigenetic mark? *Mutat Res* 647: 39–43. doi:10.1016/j.mrfmmm.2008.07.007

104. Agarwal N, Hardt T, Brero A, Nowak D, Rothbauer U, Becker A, Leonhardt H, Cardoso MC (2007) MeCP2 interacts with HP1 and modulates its heterochromatin association during myogenic differentiation. *Nucleic Acids Res* 35: 5402–5408. doi:10.1093/nar/gkm599

105. Kernohan KD, Vernimmen D, Gloor GB, Bérubé NG (2014) Analysis of neonatal brain lacking ATRX or MeCP2 reveals changes in nucleosome density, CTCF binding and chromatin looping. *Nucleic Acids Res* 42: 8356–8368. doi:10.1093/nar/gku564

106. Nan X, Ng HH, Johnson CA, Laherty CD, Turner BM, Eisenman RN, Bird A (1998) Transcriptional repression by the methyl-CpG-binding protein MeCP2 involves a histone deacetylase complex. *Nature* 393: 386–389. doi:10.1038/30764

107. Fuks F, Hurd PJ, Wolf D, Nan X, Bird AP, Kouzarides T (2003) The methyl-CpG-binding protein MeCP2 links DNA methylation to histone methylation. *J Biol Chem* 278: 4035–4040. doi:10.1074/jbc.m210256200

108. Du Q, Luu P-L, Stirzaker C, Clark SJ (2015) Methyl-CpG-binding domain proteins: Readers of the epigenome. *Epigenomics* 7: 1051–1073. doi:10.2217/epi.15.39

109. Jeffery L, Nakielny S (2004) Components of the DNA methylation system of chromatin control are RNA-binding proteins. *J Biol Chem* 279: 49479–49487. doi:10.1074/jbc.m409070200

110. Maxwell SS, Pelka GJ, Tam PP, El-Osta A (2013) Chromatin context and ncRNA highlight targets of MeCP2 in brain. *RNA Biol* 10: 1741–1757. doi:10.4161/rna.26921

111. Khan AW, Ziemann M, Rafehi H, Maxwell S, Ciccotosto GD, El-Osta A (2017) MeCP2 interacts with chromosomal microRNAs in brain. *Epigenetics* 12: 1028–1037. doi:10.1080/15592294.2017.1391429

112. Price BD, D'Andrea AD (2013) Chromatin remodeling at DNA double-strand breaks. *Cell* 152: 1344–1354. doi:10.1016/j.cell.2013.02.011

113. McDonald OG, Wu H, Timp W, Doi A, Feinberg AP (2011) Genome-scale epigenetic reprogramming during epithelial-to-mesenchymal transition. *Nat Struct Mol Biol* 18: 867–874. doi:10.1038/nsmb.2084

114. Harr JC, Reddy KL (2016) Tagged chromosomal insertion site system: A method to study lamina-associated chromatin. *Methods Enzymol* 569: 433–453. doi:10.1016/bs.mie.2015.09.028

115. Schindelin J, Arganda-Carreras I, Frise E, Kaynig V, Longair M, Pietzsch T, Preibisch S, Rueden C, Saalfeld S, Schmid B, et al (2012) Fiji: An open-source platform for biological-image analysis. *Nat Methods* 9: 676–682. doi:10.1038/nmeth.2019

116. Reddy KL, Zullo JM, Bertolino E, Singh H (2008) Transcriptional repression mediated by repositioning of genes to the nuclear lamina. *Nature* 452: 243–247. doi:10.1038/nature06727

117. Langmead B, Trapnell C, Pop M, Salzberg SL (2009) Ultrafast and memory-efficient alignment of short DNA sequences to the human genome. *Genome Biol* 10: R25. doi:10.1186/gb-2009-10-3-r25

118. Olshen AB, Venkatraman ES, Lucito R, Wigler M (2004) Circular binary segmentation for the analysis of array-based DNA copy number data. *Biostatistics* 5: 557–572. doi:10.1093/biostatistics/kxh008

119. Venkatraman ES, Olshen AB (2007) A faster circular binary segmentation algorithm for the analysis of array CGH data. *Bioinformatics* 23: 657–663. doi:10.1093/bioinformatics/btl646

120. Hsu F-H, Chen H-IH, Tsai M-H, Lai L-C, Huang C-C, Tu S-H, Chuang EY, Chen Y (2011) A model-based circular binary segmentation algorithm for the analysis of array CGH data. *BMC Res Notes* 4: 394. doi:10.1186/1756-0500-4-394